Autocorrelation function of eigenstates in chaotic and mixed systems

2002 J. Phys. A: Math. Gen. 35 539

(http://iopscience.iop.org/0305-4470/35/3/307)

INSTITUTE OF PHYSICS PUBLISHING JOURNAL OF PHYSICS A: MATHEMATICAL AND GENERAL

J. Phys. A: Math. Gen. **35** (2002) 539–564 PII: S0305-4470(02)24383-8

Autocorrelation function of eigenstates in chaotic and mixed systems

Arnd Bäcker[1,2] **and Roman Schubert**[3]

[1] School of Mathematics, University of Bristol, University Walk, Bristol BS8 1TW, UK
[2] BRIMS, Hewlett-Packard Laboratories, Filton Road, Bristol BS12 6QZ, UK
[3] Abteilung Theoretische Physik, Universität Ulm, Albert-Einstein-Allee 11, D–89069 Ulm, Germany

E-mail: a.backer@bristol.ac.uk and roman.schubert@physik.uni-ulm.de

Received 20 April 2001, in final form 14 September 2001
Published 11 January 2002
Online at stacks.iop.org/JPhysA/35/539

Abstract

We study the autocorrelation function of different types of eigenfunctions in quantum mechanical systems with either chaotic or mixed classical limits. We obtain an expansion of the autocorrelation function in terms of the correlation distance. For localized states in billiards, like bouncing ball modes or states living on tori, a simple model using only classical input gives good agreement with the exact result. In particular, a prediction for irregular eigenfunctions in mixed systems is derived and tested. For chaotic systems, the expansion of the autocorrelation function can be used to test quantum ergodicity on different length scales.

PACS numbers: 05.45.Mt, 02.50.Ey, 03.65.SQ, 05.45.−a

1. Introduction

The behaviour of a quantum mechanical system in the semiclassical limit strongly depends on the ergodic properties of the corresponding classical system. In particular, the eigenfunctions semiclassically reflect the phase space structure of the classical system and therefore they depend strongly on whether the classical system is chaotic or regular. In this study we are interested in the fluctuations of the wavefunctions, and in the correlations between the fluctuations in different regions which are induced by the classical phase space structures. In particular, we will consider the case of quantum billiards in a domain $\Omega \subset \mathbb{R}^2$, which are described by the time-independent Schrödinger equation (in units $\hbar = 2m = 1$)

$$(\Delta + E)\psi(\boldsymbol{q}) = 0 \qquad \text{for} \quad \boldsymbol{q} \in \Omega \backslash \partial\Omega \tag{1}$$

with Dirichlet boundary conditions, $\psi(\boldsymbol{q}) = 0$ for $\boldsymbol{q} \in \partial\Omega$. For compact Ω one obtains a discrete spectrum $\{E_n\}$ of eigenvalues, $0 < E_1 \leqslant E_2 \leqslant \ldots$, with associated eigenfunctions

$\psi_n \in L^2(\Omega)$, which we assume to be normalized, i.e. $\|\psi_n\| := \int_\Omega |\psi_n(\boldsymbol{q})|^2 \, \mathrm{d}q = 1$. The corresponding classical billiard is given by the free motion of a point particle inside Ω with elastic reflections at the boundary $\partial\Omega$.

The amplitude distribution of an eigenfunction of a quantum mechanical system whose classical limit is chaotic is conjectured to become Gaussian in the semiclassical limit [1], and numerical studies support this conjecture, see e.g. [2–4]. A more sensitive quantity is the *local* autocorrelation function [1] which measures correlations between different points of an eigenfunction ψ

$$C^{\mathrm{loc}}(\boldsymbol{x}, \delta\boldsymbol{x}) := \psi^*(\boldsymbol{x} - \delta\boldsymbol{x}/2)\psi(\boldsymbol{x} + \delta\boldsymbol{x}/2). \tag{2}$$

The crucial fact for the theoretical analysis of $C^{\mathrm{loc}}(\boldsymbol{x}, \delta\boldsymbol{x})$, observed by Berry [1], is that the autocorrelation function can be expressed as the Fourier transformation of the Wigner function (see equation (7) below) of ψ

$$C^{\mathrm{loc}}(\boldsymbol{x}, \delta\boldsymbol{x}) = \int W(\boldsymbol{p}, \boldsymbol{x}) \mathrm{e}^{-\mathrm{i}p\delta x} \, \mathrm{d}p. \tag{3}$$

Hence information on the behaviour of the Wigner function can be used to predict the behaviour of the autocorrelation function, and since semiclassical limits of Wigner functions are concentrated on invariant sets in phase space, see e.g. [5], it follows that in the semiclassical limit autocorrelation functions are determined by the classical phase space structure. For example, if the classical system is ergodic, the quantum ergodicity theorem [6–11] (roughly speaking) states that almost all quantum expectation values tend to the corresponding classical limit. One can show [12] that for ergodic systems this is equivalent to the semiclassical eigenfunction hypothesis [1, 13–15], when restricted to a subsequence of density one. Using this result in (3) one gets Berry's result [1] that for chaotic billiards in two dimensions

$$C^{\mathrm{loc}}(\boldsymbol{x}, \delta\boldsymbol{x}) \sim \frac{1}{\mathrm{vol}(\Omega)} J_0(\sqrt{E}|\delta\boldsymbol{x}|) \tag{4}$$

weakly as a function of $\boldsymbol{x}$ (for fixed $\delta\boldsymbol{x}$) as $E \to \infty$, where E denotes the energy of the eigenstate ψ in (2). Equivalently we have

$$\lim_{E\to\infty} C^{\mathrm{loc}}(\boldsymbol{x}, \delta\boldsymbol{x}/\sqrt{E}) = \frac{1}{\mathrm{vol}(\Omega)} J_0(|\delta\boldsymbol{x}|). \tag{5}$$

Numerical tests of this relation have been performed for several chaotic systems [2–4] and at finite energies show notable fluctuations of the autocorrelation function around the high energy limit (4), especially for correlation distances larger than a few de Broglie wavelengths.These fluctuations have been studied further in [16–19], where for a small correlation distance $|\delta\boldsymbol{x}|$ a random model for the eigenfunctions of a chaotic system was used to predict the variance of these fluctuations, and for larger $|\delta\boldsymbol{x}|$ a formula involving closed orbits of the system has been derived. In [23, 24] the path correlation function, which is an average of the local correlations along a given trajectory, has been introduced. A further study of autocorrelations of eigenfunctions in the framework of the nonlinear σ-model has been recently conducted in [20], and spectral averages of autocorelation functions are studied in [21, 22]. The path correlation function is closely related to the autocorrelation function and for ergodic systems also tends asymptotically to a Bessel function (4). This path correlation function has been studied in [3] for a hyperbolic octagon, and an expansion in terms of Legendre functions has been derived, which can be used to determine corrections to the leading Bessel part (4).

The autocorrelation function in nonchaotic systems has attracted very less attention. The integrable case has already been discussed by Berry [1], and the corresponding formula has been successfully tested for the circle billiard in [2]. For a system with mixed classical

phase space the autocorrelation function has been studied in [25], in particular for irregular eigenfunctions an expansion of the Wigner function in polar coordinates has been used.

In this paper we are interested in the question how the universal limit (4) is reached, and how, in the case of mixed systems, further constraints on the classical motion are reflected in the autocorrelation function. For instance, if an eigenfunction is concentrated on an ergodic component, then by a generalization of the quantum ergodicity theorem [26], the Wigner function becomes equidistributed on that component, and this will determine the autocorrelation function.

The paper is organized as follows. In section 2 we discuss some examples of the autocorrelation function for different eigenfunctions in systems with chaotic and mixed classical dynamics. In section 3 a general expansion of the autocorrelation function for eigenfunctions in billiards is derived, which allows a systematic study of their properties. It is an expansion in the correlation distance $|\delta \boldsymbol{x}|$ which reflects the fact that the determination of correlations at larger distances needs classical information on finer length scales than for short range correlations. In section 4 it is shown that the correlation distance expansion provides an efficient way to explain the fine structure of the autocorrelation functions of the systems studied in the first section. Of particular interest is that for chaotic systems deviations of the autocorrelation function from the quantum ergodic limit (4) can be related to the rate of quantum ergodicity. In turn the autocorrelation function can be used to study the rate of quantum ergodicity on different classical length scales.

2. Examples of autocorrelation functions

For numerical computations as well as for theoretical considerations it is much more convenient to consider a smoothed version of the local autocorrelation function (2). Furthermore, as the eigenfunctions oscillate on a scale proportional to $1/\sqrt{E}$, we rescale the autocorrelation function by this factor. Hence we will study the autocorrelation function in the form

$$C_\rho(\boldsymbol{x}, \delta \boldsymbol{x}) := \int_\Omega \rho(\boldsymbol{x}-\boldsymbol{q})\psi^*\left(\boldsymbol{q}-\frac{\delta \boldsymbol{x}}{2\sqrt{E}}\right)\psi\left(\boldsymbol{q}+\frac{\delta \boldsymbol{x}}{2\sqrt{E}}\right)\mathrm{d}q \tag{6}$$

where ρ is a positive function which determines the smoothing of the local autocorrelation function. In the literature (see the papers mentioned in the introduction) the mean is usually taken over a small disc, which corresponds to taking the characteristic function of a disc for ρ in (6). However, nothing prevents one considering the case $\rho \equiv 1$, i.e. taking the mean value of the local autocorrelation function (2) over the whole position space. In terms of the Wigner function

$$W(\boldsymbol{p}, \boldsymbol{q}) := \frac{1}{(2\pi)^2}\int \mathrm{e}^{\mathrm{i}pq'}\psi^*(\boldsymbol{q}-\boldsymbol{q}'/2)\psi(\boldsymbol{q}+\boldsymbol{q}'/2)\,\mathrm{d}q' \tag{7}$$

one obtains in this case

$$C(\delta \boldsymbol{x}) := \int \psi^*\left(\boldsymbol{q}-\frac{\delta \boldsymbol{x}}{2\sqrt{E}}\right)\psi\left(\boldsymbol{q}+\frac{\delta \boldsymbol{x}}{2\sqrt{E}}\right)\mathrm{d}q \tag{8}$$

$$= \iint W(\boldsymbol{p}, \boldsymbol{q})\mathrm{e}^{-\mathrm{i}p\delta x/\sqrt{E}}\,\mathrm{d}q\,\mathrm{d}p = \int |\hat{\psi}(\boldsymbol{p})|^2\mathrm{e}^{-\mathrm{i}p\delta x/\sqrt{E}}\,\mathrm{d}p. \tag{9}$$

This is a particularly good choice for the numerical computation of the autocorrelation function in billiards because it can be reduced to boundary integrals (see the appendix). The resulting formula reads

$$C(\delta \boldsymbol{x}) = \frac{1}{8\sqrt{E}}\iint_{\partial\Omega\times\partial\Omega} |\boldsymbol{q}(s)-\boldsymbol{q}(s')+\delta \boldsymbol{x}|\,Y_1(\sqrt{E}|\boldsymbol{q}(s)-\boldsymbol{q}(s')+\delta \boldsymbol{x}|)u^*(s)u(s')\,\mathrm{d}s\,\mathrm{d}s' \tag{10}$$

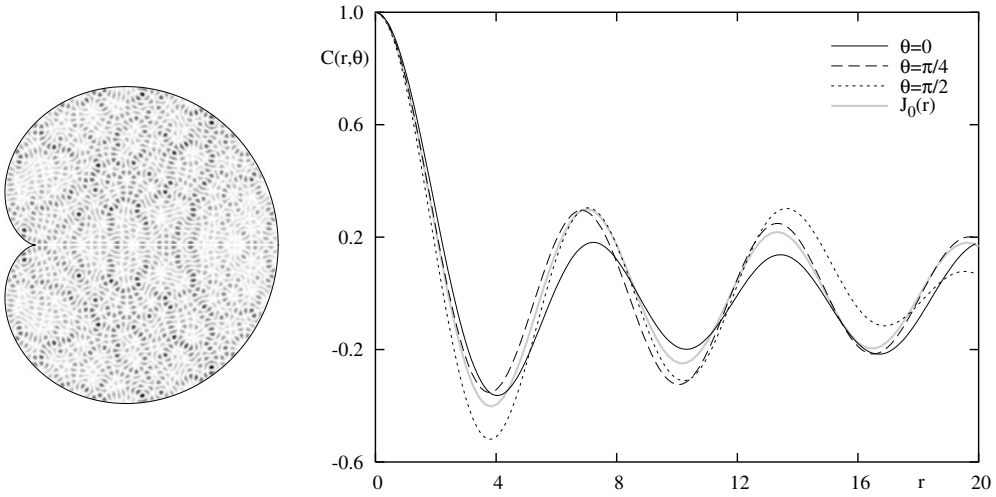

Figure 1. Grey scale plot of $|\psi_{1277}(\boldsymbol{q})|^2$ in the cardioid billiard with odd symmetry, where black corresponds to high intensity. To the right the autocorrelation function $C(r, \theta)$, computed using (10), is shown for three different directions $\theta = 0, \pi/4$ and $\pi/2$. For comparison the asymptotic result $C(r, \theta) = J_0(r)$ is shown as the grey line.

where $u(s)$ is the normal derivative of the normalized eigenfunction ψ on the billiard boundary. This relation provides a very efficient method for the numerical computation of the autocorrelation function.

The systems for which we study the autocorrelation functions are the stadium billiard and two members of the family of limaçon billiards, namely the cardioid billiard, and a billiard with mixed classical phase space. The stadium billiard is proved to be strongly chaotic, i.e. it is ergodic, mixing and a *K*-system [27, 28].The height of the desymmetrized billiard is chosen to be 1, and a denotes the length of the upper horizontal line, for which we have $a = 1.8$ in the following. The family of limaçon billiards is given by the simplest nontrivial conformal mapping of the unit circle [29, 30] and can be parametrized in polar coordinates by $\rho(\varphi) = 1 + \varepsilon\cos(\varphi)$ with $\varphi \in [-\pi, \pi]$, and $\varepsilon \in [0, 1]$ denotes the family parameter. We consider the case $\varepsilon = 0.3$ which leads to a mixed dynamics in phase space. For $\varepsilon = 1$ one obtains the cardioid billiard,which is also proved to be strongly chaotic [31–33]. The eigenvalues of the cardioid billiard have been provided by Prosen and Robnik [34] and were calculated by means of the conformal mapping technique, see e.g. [30, 35]. For the stadium billiard the eigenvalues and eigenfunctions have been computed using the boundary element method, see e.g. [36, 37], and for the limaçon billiard the eigenvalues have been computed using the conformal mapping technique and then the boundary element method has been used to compute the eigenfunctions (see [38] for details). For the high-lying states in the limaçon billiard the scaling method has been used [39].

First we consider a 'typical' eigenfunction in the cardioid billiard (figure 1). In the plots we show

$$C(r, \theta) = C(r\hat{\boldsymbol{e}}(\theta)) \tag{11}$$

where $\hat{\boldsymbol{e}}(\theta) = (\cos\theta, \sin\theta)$, as a function of r for three different values of θ .The quantum ergodicity theorem implies that there is a subsequence $\{n_j\} \subset \mathbb{N}$ of density one such that $C_{n_j}(r, \theta) \to J_0(r)$ as $n_j \to \infty$ with r fixed. This convergence is, however, not uniform in r.

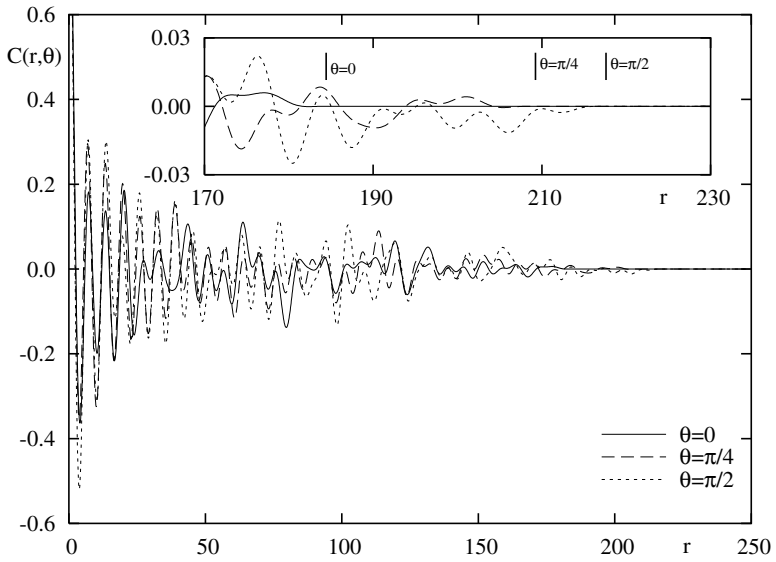

Figure 2. Autocorrelation function for the same state as figure 1, but for a larger r-interval showing the non-universal behaviour at larger r. The inset shows a magnification and the vertical bars indicate the places $r = \sqrt{E_n}\mathrm{diam}(\Omega, \theta)$ from where on $C(r, \theta) = 0$, due to the compactness of the billiard.

For the example shown in figure 1 $C(r, \theta)$ fluctuates, as expected for a 'quantum ergodic' state, around the asymptotic result

$$C(r, \theta) \sim J_0(r). \tag{12}$$

Actually, for an eigenstate with energy E_n we have $C(r, \theta) = 0$ for $r > \sqrt{E_n}\mathrm{diam}(\Omega, \theta)$, where $\mathrm{diam}(\Omega, \theta)$ is the diameter of Ω in the direction θ, as follows directly from the definition (6). This is illustrated in figure 2 which clearly shows the non-universal behaviour for larger r.

In contrast to the case of quite uniformly distributed eigenfunctions one expects a stronger directional dependence of the autocorrelation function for localized eigenfunctions, such as scars [40]. One example is shown in figure 3, where the eigenfunctions shows localization along the shortest unstable periodic orbit in the cardioid. The corresponding autocorrelation function shows clear deviations from (12).

A class of eigenfunctions which show even stronger localization are the bouncing ball modes in billiards with two parallel walls (see, e.g. [2, 41–44]). Figure 4 shows for the stadium billiard an example of a bouncing ball mode, which localizes on the so-called bouncing ball orbits having perpendicular reflections at the parallel walls and thus forming a one-parameter family. The simplest approximation is to consider them as a product of two sines, one in the x direction and the other in the y direction. In this case the autocorrelation function can be computed explicitly. For the odd–odd eigenfunctions

$$\psi_{n_x,n_y}(x, y) = \frac{1}{\sqrt{l_x l_y}} \sin(\pi n_x x/l_x) \sin(\pi n_y y/l_y) \tag{13}$$

in a box $B := [-l_x, l_x] \times [-l_y, l_y]$ one gets

$$C^{\mathrm{box}}_{n_x,n_y}(r, \theta) = F(r\cos(\theta)/\sqrt{E}, n_x, l_x)\, F(r\sin(\theta)/\sqrt{E}, n_y, l_y) \tag{14}$$

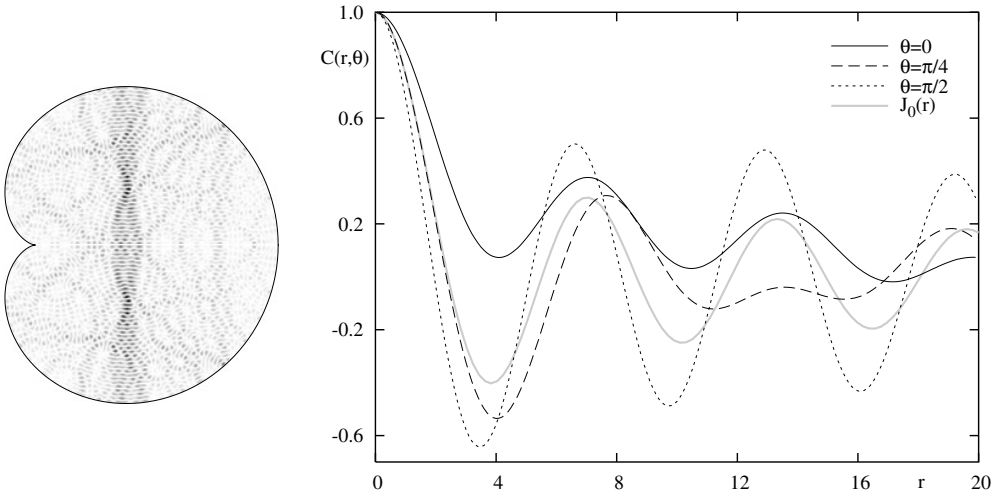

Figure 3. Grey scale plot of $|\psi_n(\boldsymbol{q})|^2$ with $n = 1277$ in the cardioid billiard with odd symmetry. For the autocorrelation function $C(r, \theta)$ one observes clear deviations from $C(r, \theta) = J_0(r)$.

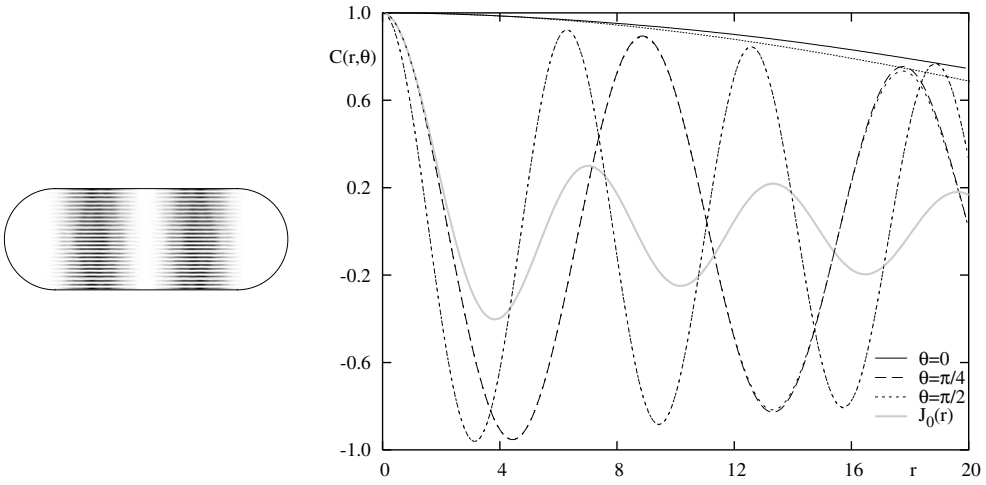

Figure 4. For the stadium billiard with odd–odd symmetry, $a = 1.8$, $\psi_{320}(\boldsymbol{q})$ is a bouncing ball mode. The corresponding autocorrelation function is compared with the result $C^{\mathrm{box}}_{1,13}(r, \theta)$, equation (14), obtained for a box, shown as dotted curves, which follow $C(r, \theta)$. Only for $\theta = 0$ (full line) and $\theta = \pi/4$ at $r \approx 17$ are small deviations visible.

where

$$F(z, n, l) := \chi_{[-l,l]}(z/2)\frac{1}{l}\int_{-l+z/2}^{l-z/2} \sin(\pi n(x - z/2)/l)\, \sin(\pi n(x + z/2)/l)\, \mathrm{d}x \tag{15}$$

$$= \chi_{[-l,l]}(z/2)\left[\left(1 - \frac{z}{2l}\right)\cos(\pi n z/l) + \frac{1}{2\pi n}\, \sin(\pi n z/l)\right] \tag{16}$$

and $\chi_{[-l,l]}(z)$ denotes the characteristic function of the interval $[-l, l]$.

In figure 4 we compare the autocorrelation $C(r, \theta)$function for a bouncing ball mode in the stadium billiard with $C^{\mathrm{box}}_{1,13}(r, \theta)$, equation (14), and observe very good agreement. Mainly

for $\theta = 0$ some deviations are visible; these are understandable from the fact that in this case only correlations in the x-direction are measured, where the bouncing ball mode 'leaks' outside the rectangular region. To take this into account one can determine an effective $l_x^{\mathrm{eff}} > 2a$, by fitting $\sin^2\left(\pi x / l_x^{\mathrm{eff}}\right)$ to

$$\psi_n^{\mathrm{proj}}(x) := \int_0^1 |\psi(x, y)|^2 \, \mathrm{d}y. \tag{17}$$

For the case shown in figure 4 this procedure leads to $l_x^{\mathrm{eff}} \approx 4$ (whereas $2a = 3.6$) and the corresponding autocorrelation function gives excellent agreement with the one for ψ_{320}.

3. Expansion of the autocorrelation function

In this section we derive an expansion of the autocorrelation function which will lead to an understanding of the directional dependence of the autocorrelation function observed in the last section. We start from the representation of the local autocorrelation function in terms of the Wigner function

$$C_\rho(\boldsymbol{x}, \delta\boldsymbol{x}) = \iint \rho(\boldsymbol{x} - \boldsymbol{q}) W(\boldsymbol{p}, \boldsymbol{q}) \mathrm{e}^{-\mathrm{i}\boldsymbol{p}\delta\boldsymbol{x}/\sqrt{E}} \, \mathrm{d}p \, \mathrm{d}q. \tag{18}$$

Since the Wigner function is concentrated around the energy shell $|\boldsymbol{p}| = \sqrt{E}$, and is furthermore even in $\boldsymbol{p}$ by time reversal symmetry, we get

$$\begin{aligned} C_\rho(\boldsymbol{x}, \delta\boldsymbol{x}) &= \int_0^\infty \int_0^{2\pi} \int_\Omega \rho(\boldsymbol{x} - \boldsymbol{q}) W(\boldsymbol{p}, \boldsymbol{q}) \, \mathrm{d}q' \, \mathrm{e}^{-\mathrm{i}|\delta\boldsymbol{x}| \cos(\varphi - \theta)} \, r \, \mathrm{d}\varphi \, \mathrm{d}r + O(|\delta\boldsymbol{x}| E^{-1/2}) \\ &= \int_0^\infty \int_0^{2\pi} \int_\Omega \rho(\boldsymbol{x} - \boldsymbol{q}) W(\boldsymbol{p}, \boldsymbol{q}) \, \mathrm{d}q \, \cos(|\delta\boldsymbol{x}| \cos(\varphi - \theta)) \, r \, \mathrm{d}\varphi \, \mathrm{d}r + O(|\delta\boldsymbol{x}| E^{-1/2}) \end{aligned} \tag{19}$$

where we have used polar coordinates $\boldsymbol{p} = (|\boldsymbol{p}| \cos\varphi, |\boldsymbol{p}| \sin\varphi)$, $\delta\boldsymbol{x} = (|\delta\boldsymbol{x}| \cos\theta, |\delta\boldsymbol{x}| \sin\theta)$. Because of the rescaling by $\sqrt{E}$ the factor $\mathrm{e}^{-\mathrm{i}\boldsymbol{p}\delta\boldsymbol{x}/\sqrt{E}}$ is only slowly oscillating for $\boldsymbol{p}$ close to the energy shell, on which the Wigner function is concentrated. Therefore we get that the error is of order $|\delta\boldsymbol{x}|/\sqrt{E}$ (see appendix B for a sketch of the derivation of this remainder estimate). If we now use that $\cos(r \cos\varphi)$ is a generating function for Bessel functions [45]

$$\cos(|\delta\boldsymbol{x}| \cos\varphi) = J_0(|\delta\boldsymbol{x}|) + 2 \sum_{l=1}^{\infty} (-1)^l \cos(2l\varphi) J_{2l}(|\delta\boldsymbol{x}|) \tag{20}$$

we obtain

$$C_\rho(\boldsymbol{x}, \delta\boldsymbol{x}) = \xi_0(\boldsymbol{x}) \, J_0(|\delta\boldsymbol{x}|) + 2 \sum_{l=1}^{\infty} (-1)^l \xi_{2l}(\boldsymbol{x}, \theta) \, J_{2l}(|\delta\boldsymbol{x}|) + O(E^{-1/2}) \tag{21}$$

with (setting $r = |\boldsymbol{p}|$)

$$\xi_{2l}(\boldsymbol{x}, \theta) := \int_0^\infty \int_0^{2\pi} \int_\Omega \rho(\boldsymbol{x} - \boldsymbol{q}) W(\boldsymbol{p}, \boldsymbol{q}) \, \mathrm{d}q \cos(2l(\varphi - \theta)) \, r \, \mathrm{d}\varphi \, \mathrm{d}r. \tag{22}$$

The coefficients $\xi_{2l}(\boldsymbol{x}, \theta)$ can be further decomposed

$$\begin{aligned} \xi_{2l}(\boldsymbol{x}, \theta) = \cos(2l\theta) &\int_0^\infty \int_0^{2\pi} \int_\Omega \rho(\boldsymbol{x} - \boldsymbol{q}) W(\boldsymbol{p}, \boldsymbol{q}) \, \mathrm{d}q \cos(2l\varphi) \, r \, \mathrm{d}\varphi \, \mathrm{d}r \\ + \sin(2l\theta) &\int_0^\infty \int_0^{2\pi} \int_\Omega \rho(\boldsymbol{x} - \boldsymbol{q}) W(\boldsymbol{p}, \boldsymbol{q}) \, \mathrm{d}q \sin(2l\varphi) \, r \, \mathrm{d}\varphi \, \mathrm{d}r. \end{aligned} \tag{23}$$

Recall that for an operator $\hat{A}$ with Weyl symbol $A(\boldsymbol{p}, \boldsymbol{q})$ the expectation value $\langle\psi, \hat{A}\psi\rangle$ can be written as an integral over the phase space of the symbol multiplied by the Wigner function of ψ, see e.g. [46],

$$\langle\psi, \hat{A}\psi\rangle = \iint W(\boldsymbol{p}, \boldsymbol{q}) A(\boldsymbol{p}, \boldsymbol{q}) \, \mathrm{d}p \, \mathrm{d}q. \tag{24}$$

Therefore the coefficients in (23) can be interpreted as expectation values of certain operators $\hat{A}_{2l}(\boldsymbol{x})$, $\hat{B}_{2l}(\boldsymbol{x})$ given as the Weyl quantizations of the functions

$$A_{2l}(\boldsymbol{p}, \boldsymbol{q}) := \rho(\boldsymbol{x} - \boldsymbol{q}) \cos(2l\varphi) \qquad B_{2l}(\boldsymbol{p}, \boldsymbol{q}) = \rho(\boldsymbol{x} - \boldsymbol{q}) \sin(2l\varphi) \tag{25}$$

respectively,

$$\int_\Omega \int_0^{2\pi} \int_0^\infty W(\boldsymbol{p}, \boldsymbol{q}) \, \rho(\boldsymbol{x} - \boldsymbol{q}) \cos(2l\varphi) \, r \, \mathrm{d}r \, \mathrm{d}\varphi \, \mathrm{d}q = \langle\psi, \hat{A}_{2l}(\boldsymbol{x})\psi\rangle \tag{26}$$

$$\int_\Omega \int_0^{2\pi} \int_0^\infty W(\boldsymbol{p}, \boldsymbol{q}) \, \rho(\boldsymbol{x} - \boldsymbol{q}) \sin(2l\varphi) \, r \, \mathrm{d}r \, \mathrm{d}\varphi \, \mathrm{d}q = \langle\psi, \hat{B}_{2l}(\boldsymbol{x})\psi\rangle. \tag{27}$$

Note that the operators $\hat{A}_{2l}(\boldsymbol{x})$ and $\hat{B}_{2l}(\boldsymbol{x})$ depend on the parameter $\boldsymbol{x}$. Since their symbols are smooth and homogeneous of degree zero in $\boldsymbol{p}$ they are classical pseudodifferential operators of order zero, see e.g. [46] for the definition of pseudodifferential operators. So we finally obtain the following general expansion of the autocorrelation function

$$\begin{aligned} C_\rho(\boldsymbol{x}, \delta\boldsymbol{x}) = \langle\psi, \hat{A}_0(\boldsymbol{x})\psi\rangle \, J_0(|\delta\boldsymbol{x}|) + 2\sum_{l=1}^{\infty}(-1)^l [\langle\psi, \hat{A}_{2l}(\boldsymbol{x})\psi\rangle \cos(2l\theta) \\ + \langle\psi, \hat{B}_{2l}(\boldsymbol{x})\psi\rangle \sin(2l\theta)] \, J_{2l}(|\delta\boldsymbol{x}|) + O(|\delta\boldsymbol{x}|E^{-1/2}) \end{aligned} \tag{28}$$

in terms of the expectation values of a sequence of bounded operators given as Weyl quantizations of the symbols (25). Recall that the only approximation we have made was to insert for $|\boldsymbol{p}|$ in the exponent in equation (19) the value at the energy shell $\sqrt{E}$.

Since the Bessel functions have the property that $J_{2l}(|\delta\boldsymbol{x}|) \approx 0$ for $|\delta\boldsymbol{x}| \ll 2l$, this representation is an efficient expansion for small $|\delta\boldsymbol{x}|$, then only a few terms in the sum contribute. But the larger $|\delta\boldsymbol{x}|$ becomes, the more terms of the sum have to be taken into account. Therefore it is desirable to have an estimate of the number of terms which have to be taken into account for large $|\delta\boldsymbol{x}|$. The first, and largest, maximum of $J_{2l}(r)$ lies around $r \sim 2l$, and close to it one has the expansion [45]

$$J_{2l}(2l - zl^{1/3}) = \frac{1}{l^{1/3}}\mathrm{Ai}(z) + O(1/l). \tag{29}$$

So the first peak becomes broader with a rate $\sim l^{1/3}$ and therefore we have to take for large r approximately

$$m \sim \frac{r}{2} + \frac{z}{2}\left(\frac{r}{2}\right)^{1/3} \tag{30}$$

terms in the sum over l into account; here z determines the error term. We refer to appendix C for a more detailed discussion.

We would like to mention two papers in which related results have been obtained. For the case of a free particle on a surface of constant negative curvature an expansion of the path correlation function in terms of the Legendre function was derived in [3]. In the special case of averaging over the whole billiard (i.e. $\rho = 1$) the path correlation function for ergodic systems should be the same as the autocorrelation function. In [25] an expansion similar to (28) was derived for the case when the eigenfunction is concentrated on an ergodic component of the phase space of a classically mixed system, however, without extracting the Bessel function

from the expectation values. To make this possible is the main reason why we have restricted our attention here to billiards. For more general systems one could derive similar expansions which approximate the autocorrelation function for small correlation distances using only a few terms, but their structure becomes more complicated.

The correlation distance expansion (28) has various possible applications; some of them will be discussed and illustrated in the next section. In particular, the expansion leads to a prediction for the asymptotic limit of the autocorrelation function in different situations. More precisely, consider a subsequence of eigenfunctions $\{\psi_{n_j}\}_{j\in\mathbb{N}}$ for which the corresponding sequence of Wigner functions converges weakly to a measure ν on phase space. Such a measure ν is called a quantum limit, and it is an invariant measure of the classical flow [5].

If a sequence of eigenfunctions $\{\psi_{n_j}\}_{j\in\mathbb{N}}$ converges to a quantum limit, the correlation distance expansion for the autocorrelation function (28) shows that the corresponding sequence of autocorrelation functions converges as well and their limit is obtained by substituting in (28) the expectation values of $\hat{A}_{2l}(\boldsymbol{x})$ and $\hat{B}_{2l}(\boldsymbol{x})$ by their corresponding classical limit. Explicitly, this gives

$$C_\rho^{\text{limit}}(\boldsymbol{x},\delta\boldsymbol{x}) = \bar{A}_0 J_0(|\delta\boldsymbol{x}|) + 2\sum_{l=1}^{\infty}(-1)^l[\bar{A}_{2l}(\boldsymbol{x})\,\cos(2l\theta) + \bar{B}_{2l}(\boldsymbol{x})\,\sin(2l\theta)]\,J_{2l}(|\delta\boldsymbol{x}|) \quad (31)$$

where

$$\bar{A} := \int_{T^*\Omega} A\,\mathrm{d}\nu. \quad (32)$$

As we will discuss in section 4.4, for ergodic systems almost all eigenfunctions have the Liouville measure as the quantum limit, then the terms $\bar{A}_{2l}$ and $\bar{B}_{2l}$ vanish, and with $\bar{A}_0 = 1$ we recover (12).

4. Applications of the correlation distance expansion

4.1. Direct comparison

In the numerical examples we have studied the autocorrelation function in the case $\rho = 1$, which allows for an exact computation of the autocorrelation function using the representation (10), which is much more efficient than a direct computation of the autocorrelation function by its definition, equation (8). In this case the general expansion (28) gives the representation

$$C(r,\theta) = J_0(r) + 2\pi\sum_{l=1}^{\infty}(-1)^l[a_{2l}\cos(2l\theta) + b_{2l}\sin(2l\theta)]\,J_{2l}(r) + O(rE^{-1/2}) \quad (33)$$

where the coefficients a_{2l} and b_{2l} are the Fourier coefficients

$$a_{2l} = \frac{1}{\pi}\int_0^{2\pi} I(\varphi)\cos(2l\varphi)\,\mathrm{d}\varphi \qquad b_{2l} = \frac{1}{\pi}\int_0^{2\pi} I(\varphi)\sin(2l\varphi)\,\mathrm{d}\varphi \quad (34)$$

of the radially integrated momentum density [47, 48]

$$I(\varphi) := \int_0^{\infty} |\hat{\psi}(r\boldsymbol{e}(\varphi))|^2 r\,\mathrm{d}r \quad (35)$$

where $\boldsymbol{e}(\varphi) = (\cos\varphi, \sin\varphi)$. Also for $I(\varphi)$ a representation in terms of a double integral of the normal derivative function is available [48]. Taking the symmetries into account, one can show that for the odd eigenfunctions in the limaçon billiards and the odd–odd eigenfunctions in the stadium billiard all b_{2l} vanish, so only the cosine terms remain in (28) and (33).

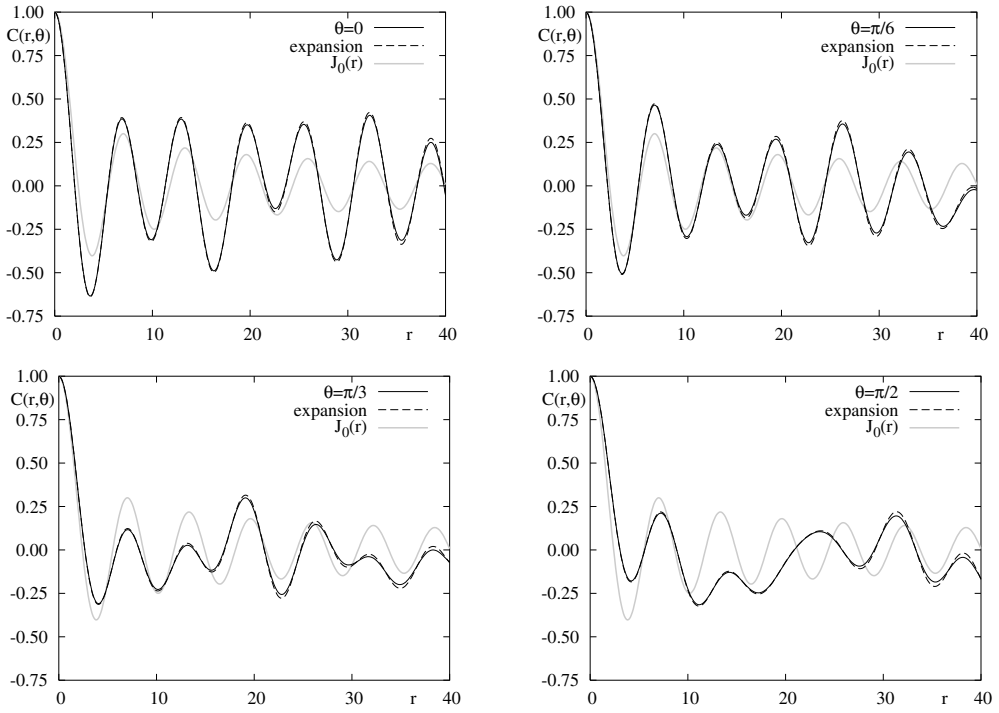

Figure 5. Comparison of the autocorrelation function $C(r, \theta)$ for ψ_{1907} in the stadium billiard (full curve) with the expansion (33). In particular, for small r the agreement is excellent, whereas for larger r small differences become visible.

First we will test the influence of the error term $O(E^{-1/2})$ in equation (33) for computations at finite energies. To that end we use the exact quantum $I(\varphi)$ in equation (34). In figure 5 the autocorrelation function $C(r, \theta)$ for four different angles θ is compared to (33). In particular, for r not too big the agreement is excellent. Only for larger r do small deviations become visible, which go to zero for higher energies and r fixed. One should remark that for any $r > 0$ the effective integration region in equation (8) is reduced by the factor

$$c(r, \theta) := \frac{\mathrm{vol}(\Omega \cap \Omega(r/\sqrt{E}, \theta))}{\mathrm{vol}(\Omega)} \tag{36}$$

where $\Omega(r/\sqrt{E}, \theta)$ is the set Ω shifted by the vector $r/\sqrt{E}$ $(\cos\theta, \sin\theta)$. Incorporating this factor leads to an improvement in the agreement of the expansion with the exact autocorrelation function at larger r.

Instead of looking at the dependence of the autocorrelation function $C(r, \theta)$ for fixed θ and varying r, it is also interesting to keep r fixed and consider the angular dependence. For a 'chaotic' eigenfunction in the cardioid billiard some examples are shown in figure 6. The result of the expansion (33) is in good agreement with the exact result. For larger r the autocorrelation function $C(r, \theta)$ oscillates more strongly around $J_0(r)$. For even larger r we observe clear deviations of the expansion from the exact result (not shown). For comparison

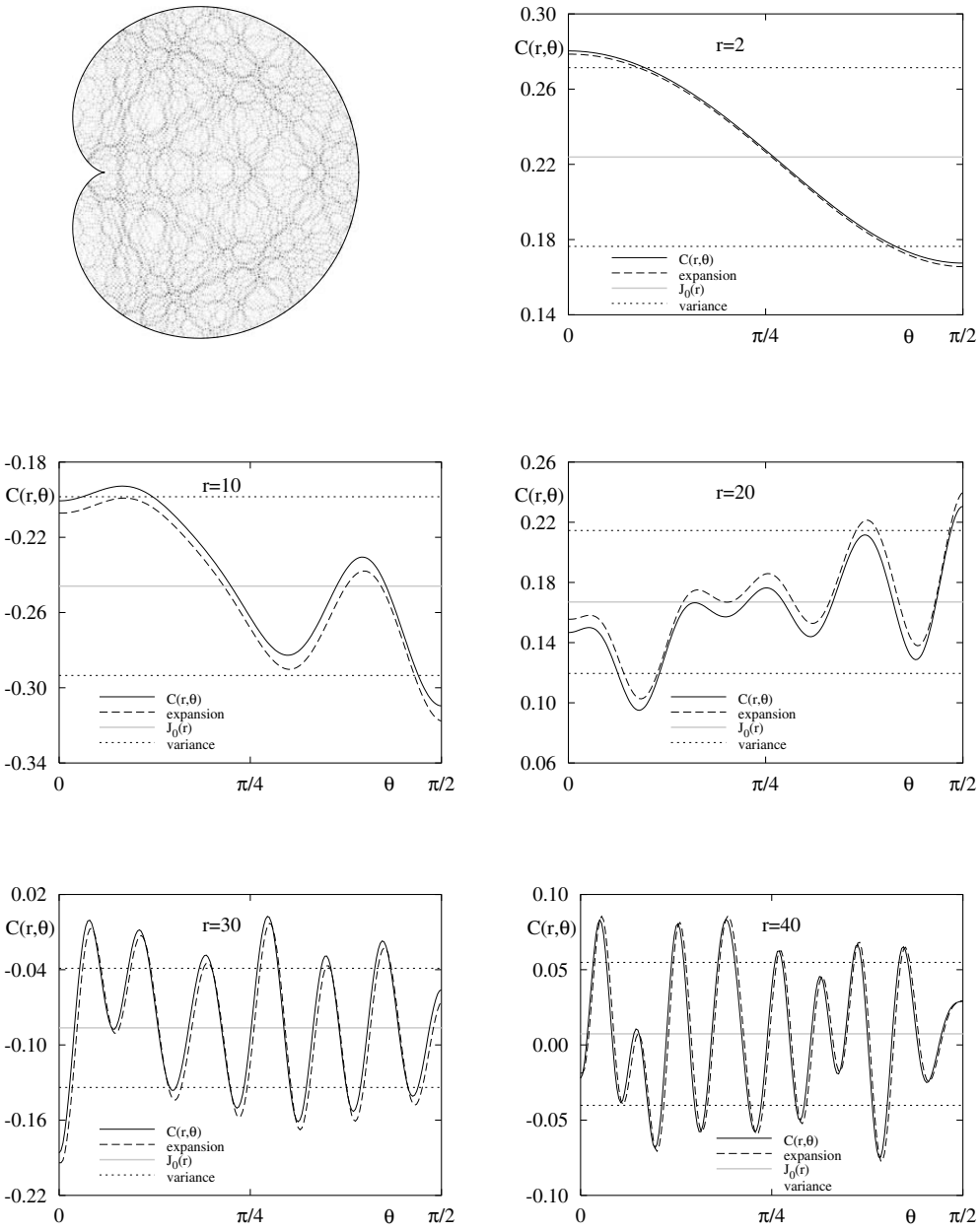

Figure 6. Angular dependence of the autocorrelation function $C(r, \theta)$ for different r. Shown are the results for ψ_{6000} in the cardioid billiard with odd symmetry. The full line is the result for $C(r, \theta)$ using (10), the dashed line shows the result of the expansion (33), the full grey line is the value of $J_0(r)$ and the dotted horizontal lines show the variance $J_0(r) \pm \Delta^{1/2}$ (see equation (37)).

the variance of the autocorrelation function around the prediction $J_0(r)$ for a random wave model [16] in leading order

$$\Delta^{1/2} = \left(\frac{16}{3\pi^{3/2}A}\right)^{1/2} \frac{1}{E^{1/4}} \tag{37}$$

is shown and good agreement is found. Note that for bounded r this error is much larger than the additional error term $O(rE^{-1/2})$ from (33).

4.2. Localized eigenfunctions

For a state strongly localized on an periodic orbit of length l_γ we have (either in the semiclassical limit, or as a crude model at finite energies)

$$I(\varphi) \sim \frac{1}{l_\gamma} \sum l_{\gamma_i} \delta(\varphi - \varphi_i) \tag{38}$$

where l_{γ_i} are the lengths of the segments of the orbit with direction φ_i. Thus we get

$$a_{2l} = \frac{1}{\pi l_\gamma} \sum l_{\gamma_i} \cos(2l\varphi_i) \qquad b_{2l} = \frac{1}{\pi l_\gamma} \sum l_{\gamma_i} \sin(2l\varphi_i) \tag{39}$$

which therefore using (33) gives a prediction for $C(\delta \boldsymbol{x})$ for such states, namely

$$C(\delta \boldsymbol{x}) \sim \frac{1}{l_\gamma} \sum_i l_{\gamma_i} \cos(|\delta \boldsymbol{x}| \cos(\theta - \varphi_i)). \tag{40}$$

Note that in the presence of symmetries all symmetry-related directions have to be taken into account in equation (38). For this simple model one can determine the autocorrelation function more directly by using (3)

$$\begin{aligned} C(\delta \boldsymbol{x}) &= \iint W(\boldsymbol{p}, \boldsymbol{q}) \mathrm{e}^{\mathrm{i}\boldsymbol{p}\delta\boldsymbol{x}} \, \mathrm{d}p \, \mathrm{d}q = \int |\hat{\psi}(\boldsymbol{p})|^2 \mathrm{e}^{\mathrm{i}\boldsymbol{p}\delta\boldsymbol{x}} \, \mathrm{d}p \\ &= \int_0^{2\pi} I(\varphi) \cos(|\delta \boldsymbol{x}| \cos(\theta - \varphi)) \, \mathrm{d}\varphi + O(|\delta \boldsymbol{x}| E^{-1/2}) \end{aligned} \tag{41}$$

inserting (38) directly gives (40).

In figure 7 we compare the limiting behaviour (40) with the autocorrelation function of a high-lying eigenstate in the limaçon billiard. The state localizes on the (stable) orbit of triangular shape. Up to $r \approx 10$ the agreement is very good; for larger r the autocorrelation function of the eigenstate shows deviations from the asymptotic behaviour. Note that the state has a much higher energy than the other examples. At lower energies the agreement is not as good, because the region in phase space on which the state localizes is broader. This in turn implies that its corresponding radially integrated momentum distribution $I(\varphi)$ also has broad peaks, which are not accounted for properly by the ansatz (38). However, when considering states of this type with increasing energies, a clear trend to the asymptotic result (40) is observed.

This simple model has also been tested for a scarred state in the cardioid. However, the agreement is limited to a qualitative description for up to $r \approx 2$. This is understandable in view of the observation (see [48, figure 8(a)]) that for a scarred state the radially integrated momentum distribution $I(\varphi)$ shows quite large fluctuations, and also in the considered case the direction $\varphi = \pi/2$ is not clearly pronounced. As these fluctuations essentially correspond to the random 'background' fluctuations of the state, a simple ansatz to model this behaviour is

$$C(r, \theta) = (1 - \alpha) J_0(r) + \alpha \frac{1}{l_\gamma} \sum_i l_{\gamma_i} \cos(|\delta \boldsymbol{x}| \cos(\theta - \varphi_i)). \tag{42}$$

It turns out that one can vary α such that quite good agreement of this model with the exact autocorrelation function is obtained (see figure 8 where $\alpha = 0.22$ (for all directions)). Depending on the direction θ the 'optimal' value for α does vary, which already indicates the limitations of this simple model. To get a better agreement a more precise description of

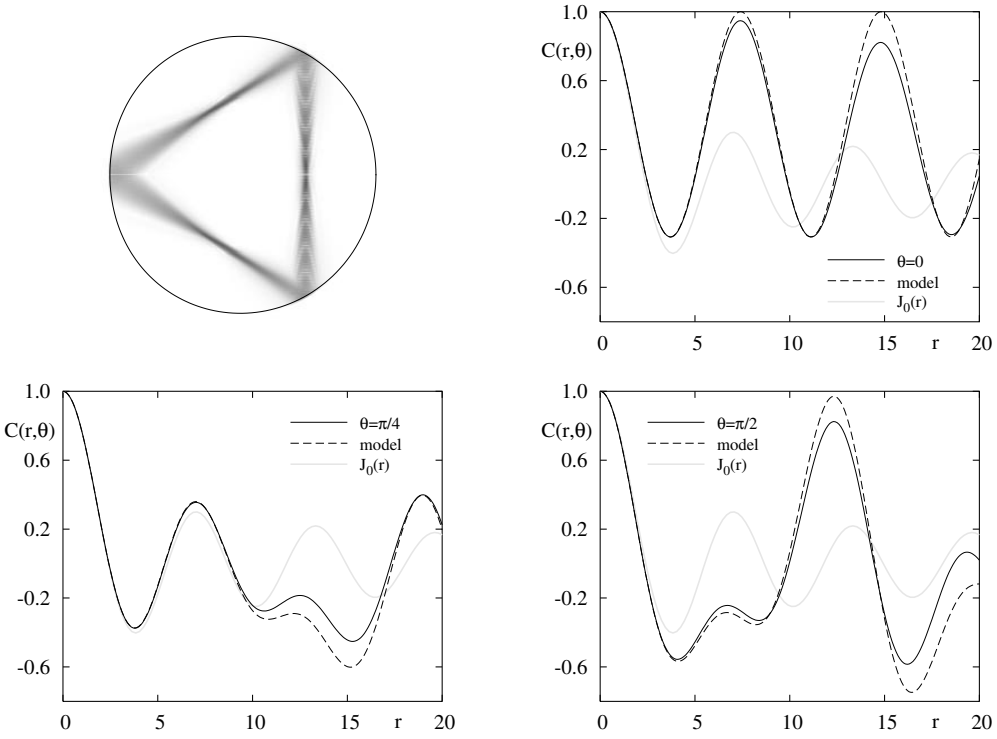

Figure 7. High-lying eigenfunction ($E = 367\,984.82\ldots$, approx. 47 788th eigenfunction of odd symmetry) in the limaçon billiard ($\varepsilon = 0.3$), which localizes on the stable orbit of triangular shape. The autocorrelation function for three different directions is compared with the δ-model, equation (40), shown as the dashed line using the directions of the stable orbit.

$I(\varphi)$ for scarred states is necessary. In particular, this should also lead to an understanding of the energy dependence of α which is expected to go to zero in the semiclassical limit. Note that the structure of the autocorrelation function is quite similar to the one for ψ_{1817} shown in figure 3.

Another case, for which we obtain much better agreement, is for an eigenfunction localized on an invariant torus. In such a case the expectation values, equations (26), (27), tend to the mean of the classical observable over the torus (see equations (31), (32)). Figure 9(*a*) shows for the limaçon billiard the eigenfunction and the corresponding Husimi Poincaré representation [49, 50]; see [51] for a more detailed discussion and the formula which has been used. Also shown in the Husimi plot are the points of some orbits. Using an initial condition on the torus we can determine the classical angular distribution $I^{\text{classical}}(\varphi)$. As this has a singularity due to the caustic of the torus we show in figure 9(*c*) a binned distribution together with the corresponding quantum radially integrated momentum distribution $I_{3056}(\varphi)$. There is qualitative agreement between these two curves in the sense that smoothing $I^{\text{classical}}(\varphi)$ describes the mean behaviour of the quantum $I_{3056}(\varphi)$. Of course, the classical distribution cannot describe the (quantum) oscillations visible for $I_{3056}(\varphi)$. It turns out, see figures 9(*d*)–(*f*), that already this simple model leads to surprisingly good agreement between the exact autocorrelation function and the expansion (33) computed using $I^{\text{classical}}(\varphi)$.

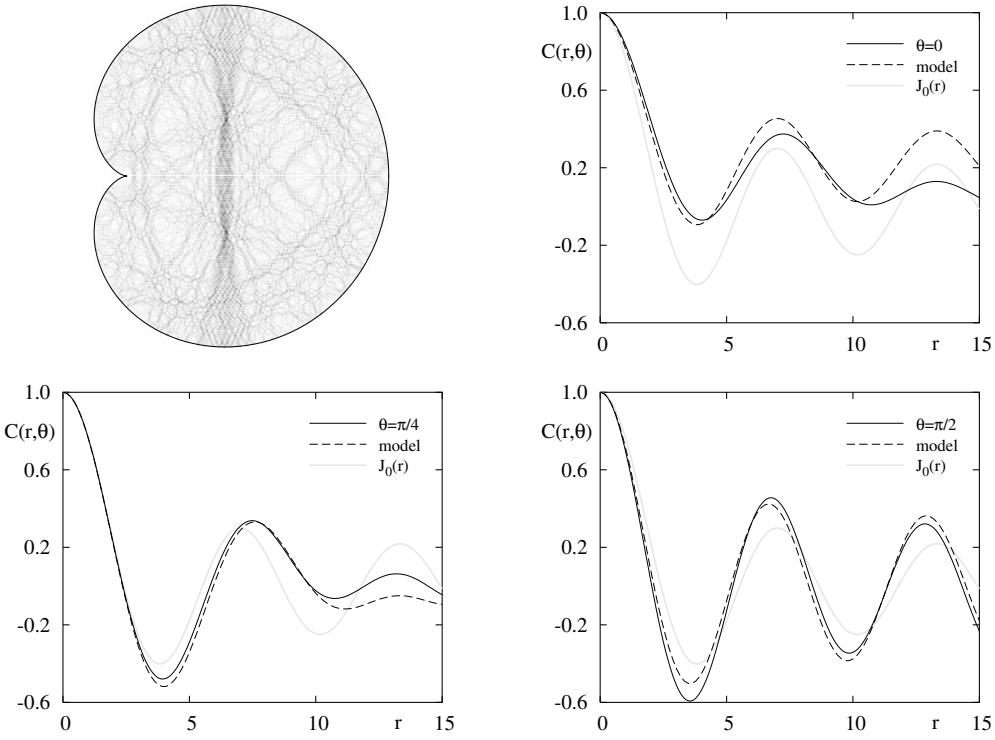

Figure 8. For a scarred state (ψ_{7147} of odd symmetry) in the cardioid billiard the autocorrelation function is compared with the simple model (42) for $\alpha = 0.22$.

4.3. Autocorrelation function of irregular states in mixed systems

In classical systems with mixed phase space regions with regular and regions with stochastic behaviour coexist. It is conjectured [52] that correspondingly the quantum mechanical eigenfunctions split into regular and irregular ones, respectively, living semiclassically on the corresponding parts of phase space. This has been confirmed numerically for several systems (see e.g. [53–57]). Consider now a sequence of eigenfunctions ψ_{n_j} which localize on some open ergodic domain D in a system with mixed phase space, then almost all the expectation values $\langle \psi_{n_j} \hat{A} \psi_{n_j} \rangle$ tend to the mean $\bar{A}^D$ of the corresponding classical observable A over this domain D [26]. Therefore using (33) we get in the limit $E \to \infty$ for the autocorrelation function of such a sequence

$$C_\rho^{\text{limit}}(\boldsymbol{x}, \delta\boldsymbol{x}) = \bar{A}_0^D J_0(|\delta\boldsymbol{x}|) + 2\sum_{l=1}^{\infty}(-1)^l \left[\bar{A}_{2l}^D(\boldsymbol{x})\cos(2l\theta) + \bar{B}_{2l}^D(\boldsymbol{x})\sin(2l\theta)\right] J_{2l}(|\delta\boldsymbol{x}|). \tag{43}$$

Instead of computing $\bar{A}_{2l}^D$ and $\bar{B}_{2l}^D$ directly, we can also use a typical trajectory of the ergodic component to determine the corresponding classical $I^{\text{classical}}(\varphi)$ via

$$I^{\text{classical}}(\varphi) = \lim_{l\to\infty} \frac{1}{l} \sum l_i \delta(\varphi - \varphi_i) \tag{44}$$

where l is the total length of the trajectory and φ_i is the direction of the ith segment having length l_i. Then we use (33) to get a prediction for the autocorrelation function.

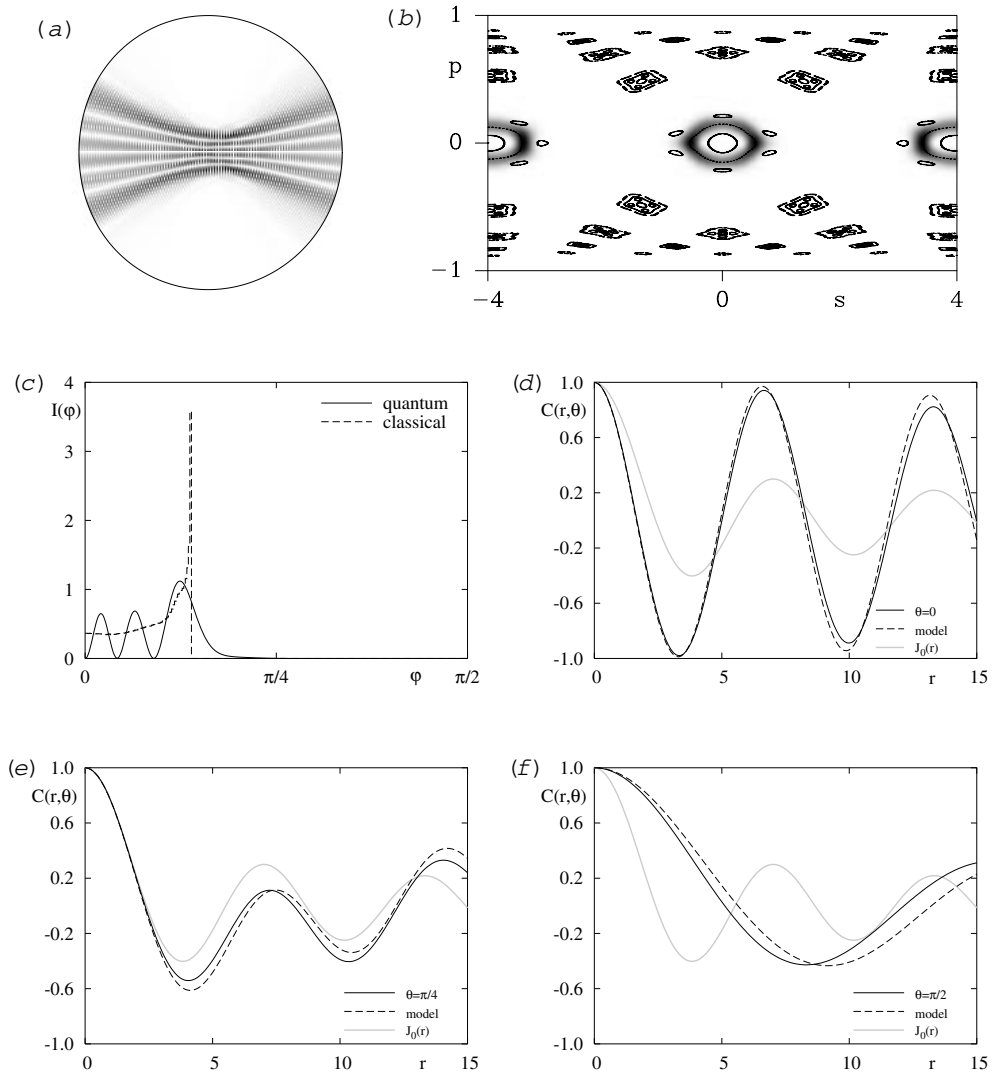

Figure 9. Grey scale plot of ψ_{3056} for the limaçon billiard with $\varepsilon = 0.3$ together with the corresponding Husimi plot, for which in addition some orbits are shown. In (*c*) the radially integrated momentum distribution $I_{3056}(\varphi)$ and the corresponding classical distribution $I^{\text{classical}}(\varphi)$ for the torus are shown. In (*d*)–(*f*) the exact autocorrelation function is compared with the expansion of the autocorrelation function, equation (33), using $I^{\text{classical}}(\varphi)$ for different angles θ.

However, we observe that even quite high-lying states do not yet localize on the whole chaotic component. Instead they are confined to smaller subregions due to partial barriers in phase space. Figure 10(*a*) shows an example of a high-lying state in the limaçon billiard ($\varepsilon = 0.3$) In figure 10(*b*) the corresponding Husimi function is plotted, which clearly shows the localization on a chaotic subdomain (the whole irregular region is much larger). If D is an open region in phase space, then the corresponding classical distribution of the momentum directions is given by

$$I^{\text{classical}}(\varphi) = \frac{1}{\text{vol}(D)} \int \chi_D(\boldsymbol{p}(\varphi), \boldsymbol{q})\, \mathrm{d}q \tag{45}$$

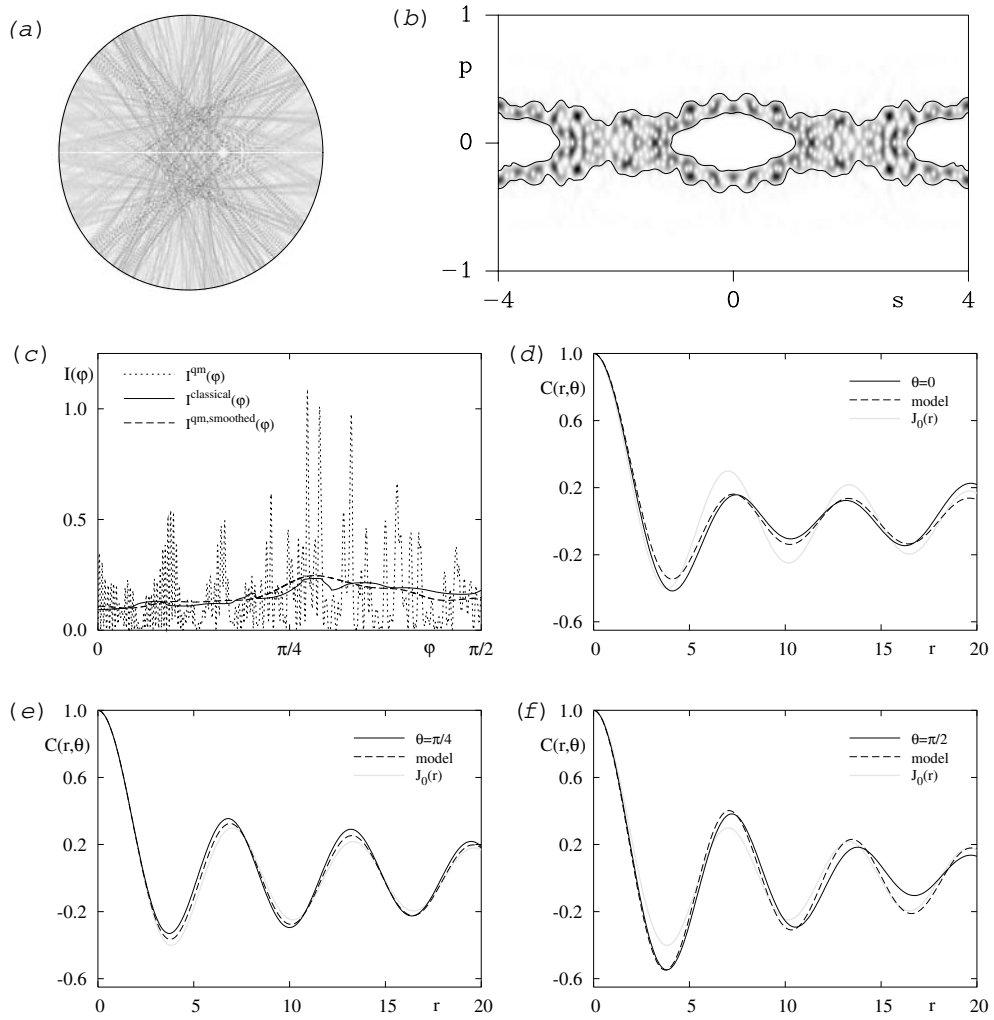

Figure 10. Autocorrelation function for a high-lying irregular state ($E = 1002\,754.70\ldots$, approx. 130 516th eigenfunction of odd symmetry) in the limaçon billiard with $\varepsilon = 0.3$. In (*b*) the Husimi representation on the boundary is shown together with an approximate boundary (full curve) of the region $\mathcal{D}$ on which the state localizes. The resulting classical momentum distribution $I^{\text{classical}}(\varphi)$ is shown in (*c*) as a full curve and compared with the radially integrated momentum distribution $I^{\text{qm}}(\varphi)$ of the state in (*a*) and a smoothing of this, $I^{\text{qm,smoothed}}(\varphi)$, shown as a dashed curve. In (*d*)–(*f*) the autocorrelation function $C(r, \theta)$ of the eigenfunction is compared for three different directions with result of the expansion (43) using $I^{\text{classical}}(\varphi)$.

where $\boldsymbol{p}(\varphi) = (\cos\varphi, \sin\varphi)$. One can show that in terms of the projection $\mathcal{D}$ of D on the Poincaré section this equation can be reduced to

$$I^{\text{classical}}(\varphi) = \frac{\int_{\mathcal{D}} l(s,p)\delta(\varphi - \phi(s,p))\,\mathrm{d}s\,\mathrm{d}p}{\int_{\mathcal{D}} l(s,p)\,\mathrm{d}s\,\mathrm{d}p} \tag{46}$$

$$= \frac{\int_{\partial\Omega'(\varphi)} l(s,p(s,\varphi))\sqrt{1-p^2(s,\varphi)}\,\chi_{\mathcal{D}}(s,p(s,\varphi))\,\mathrm{d}s}{\int_{\mathcal{D}} l(s,p)\,\mathrm{d}s\,\mathrm{d}p} \tag{47}$$

where $l(s, p)$ is the length of the orbit segment starting in the point $(s, p) \in \mathcal{P}$ with direction $\phi(s, p)$ and in the second equation $p(s, \varphi) = \boldsymbol{p}(\varphi)\boldsymbol{t}(s)$, with $\boldsymbol{t}(s)$ denoting the unit tangent vector to ∂D at the point s. Furthermore, $\partial\Omega'(\varphi) := \{s \in \partial\Omega \mid \boldsymbol{p}(\varphi)\boldsymbol{n}(s) \leqslant 0\}$, where $\boldsymbol{n}(s)$ denotes the outer normal vector to ∂D in the point s, is the subset of $\partial\Omega$ where the vector $\boldsymbol{p}(\varphi)$ points inwards. For the numerical computation we have used (47) because we just have to deal with a one-dimensional integral to compute the φ dependence, and also compared to (46) no binning of $I^{\text{classical}}(\varphi)$ is necessary.

After these general remarks on the computation of $I^{\text{classical}}(\varphi)$ let us describe how we compute the relevant quantities to determine the autocorrelation function for the state shown in figure 10(*a*). To describe the projection $\mathcal{D}$ of the domain D in phase space, we use an approximation of the boundary of $\mathcal{D}$ by a splines, which are shown in the figure 10(*b*) as full curves. Then we use equation (47) to determine the corresponding $I^{\text{classical}}(\varphi)$, shown in (*c*) as a full curve. Of course the radially integrated momentum distribution $I^{\text{qm}}(\varphi)$ of the eigenstate shows strong fluctuations, but the smoothing $I^{\text{qm,smoothed}}(\varphi)$ is well described by $I^{\text{classical}}(\varphi)$, although the agreement is not perfect. Using $I^{\text{classical}}(\varphi)$ we employ the expansion (43) to get a prediction for the autocorrelation function for states localizing on $\mathcal{D}$, which is compared in figures 10(*d*)–(*f*) with the exact autocorrelation function. Up to $r \approx 10$ we get quite good agreement, whereas for larger r deviations become more visible. This shows that the eigenfunction has more structure than accounted for by $I^{\text{classical}}(\varphi)$, i.e. it is not yet far enough in the semiclassical limit.

For higher energies the states tend to localize on the full ergodic region, and then $I^{\text{classical}}(\varphi)$ can simply be computed using (44) by averaging a typical trajectory in D. One should emphasize that the agreement has to be compared with the agreement of the autocorrelation function for ergodic systems with (12) as the prediction equation (43) only takes into account the classical limit. This has been studied in [25] (in the case of averaging the local autocorrelation function over a small disc), where in particular for [25, figure 13(*b*)] very good agreement has been found.

4.4. Ergodic systems and the rate of quantum ergodicity

If the classical billiard is ergodic, then by the quantum ergodicity theorem [6–11] almost all eigenfunctions become equidistributed in the semiclassical limit. More precisely, there exists a subsequence $\{\psi_{n_j}\}_{j\in\mathbb{N}}$ of density one, i.e. $\lim_{E\to\infty} \frac{\#\{E_{n_j} \leqslant E\}}{\#\{E_n \leqslant E\}} = 1$, such that

$$\lim_{j\to\infty} \langle \psi_{n_j}, \hat{A}\psi_{n_j} \rangle = \bar{A} \tag{48}$$

for all pseudodifferential operators $\hat{A}$, and $\bar{A}$ denotes the mean with respect to the Liouville measure of the corresponding classical observable. The rate by which this equidistribution is reached is called the rate of quantum ergodicity. It is an important quantity, as it determines the practical applicability of the quantum ergodicity theorem at finite energies.

If the billiard is ergodic and ψ_{n_j} is a quantum ergodic sequence of eigenfunctions, then for $j \to \infty$

$$\langle \psi_{n_j}, \hat{A}_{2l}(\boldsymbol{x})\psi_{n_j} \rangle \sim \bar{A}_{2l} = \delta_{l0} \tag{49}$$

$$\langle \psi_{n_j}, \hat{B}_{2l}(\boldsymbol{x})\psi_{n_j} \rangle \sim \bar{B}_{2l} = 0. \tag{50}$$

Thus using the expansion (28) we again get (12) for $E \to \infty$. Deviations from this universal behaviour are then determined by the rate at which the limit in (49) and (50) is reached, i.e. the

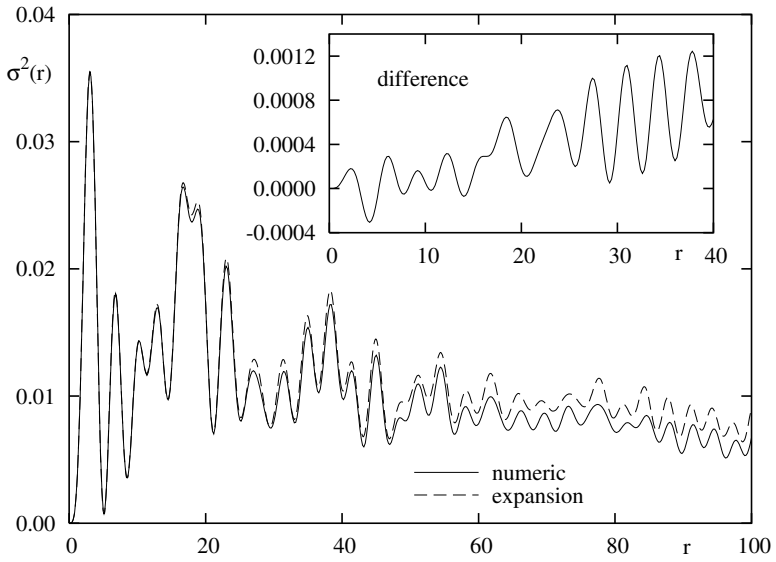

Figure 11. Comparison of the second moment $\sigma^2{}_{1907}(r)$ of the autocorrelation function, equation (52), with the expansion (53) for the stadium billiard. The inset shows the difference for $r \in [0, 20]$.

rate of quantum ergodicity. In order to exploit this it will be convenient to remove the angular dependence by taking the mean over all angular directions in $C(\delta\boldsymbol{x})$. Since by equation (33)

$$\frac{1}{2\pi}\int_0^{2\pi} C_n(r,\theta)\,\mathrm{d}\theta = J_0(r) + O(rE^{-1/2}) \tag{51}$$

we consider the second moment

$$\sigma_n^2(r) := \frac{1}{2\pi}\int_0^{2\pi} [C_n(r,\theta) - J_0(r)]^2\,\mathrm{d}\theta \tag{52}$$

where $C_n(r,\theta)$ denotes the autocorrelation function of ψ_n. Inserting the expansion (33) of $C_n(\delta\boldsymbol{x})$ leads to

$$\sigma_n^2(r) = 2\pi^2 \sum_{l=1}^{\infty} \left(a_{2l,n}^2 + b_{2l,n}^2\right) [J_{2l}(r)]^2\,(1 + O(rE^{-1/2})). \tag{53}$$

In figure 11 we compare $\sigma^2(r)$ for an eigenfunction in the stadium billiard with the expansion (53). For small r we get excellent agreement and some deviations become visible in the plot for $r > 20$. The inset shows a plot of the difference up to $r = 20$. It is surprising that even though for large r the amplitudes do not match anymore, still the expansion gives the right oscillatory structure.

If we take the mean of (53) over all eigenfunctions up to energy E, we get

$$\bar{\sigma}^2(E,r) := \frac{1}{N(E)} \sum_{E_n \leqslant E} \sigma_n^2(r) \tag{54}$$

$$= 2\pi^2 \sum_{l=1}^{\infty} \frac{1}{N(E)} \sum_{E_n \leqslant E} \left(a_{2l,n}^2 + b_{2l,n}^2\right)\ [J_{2l}(r)]^2\,(1 + O(rE^{-1/2})). \tag{55}$$

Remarkably, together with equations (28) and (53) this shows that the rate of quantum ergodicity can be studied in terms of the autocorrelation function. Particularly interesting is

that the observables in the expansion (28) become more and more oscillatory with increasing l, so by varying $|\delta \boldsymbol{x}|$ one can determine the rate of quantum ergodicity on different length scales.

A prediction for the behaviour of $\bar{\sigma}^2(E, r)$ follows from [58], where it is argued that (under suitable conditions on the system) in the mean

$$\frac{1}{N(E)} \sum_{E_n \leqslant E} \left[\langle \psi_{n_j}, \hat{A} \psi_{n_j} \rangle - \bar{A} \right]^2 \sim \frac{4\sigma_{\mathrm{cl}}^2(A)}{\mathrm{vol}\,\Omega} \frac{1}{\sqrt{E}} \tag{56}$$

for any pseudodifferential operator $\hat{A}$ of order zero with symbol A. Here $\bar{A}$ denotes the mean value of A, and $\sigma_{\mathrm{cl}}^2(A)/\sqrt{T}$ is the variance of the fluctuations of

$$\frac{1}{T} \int_0^T A(\boldsymbol{p}(t), \boldsymbol{q}(t))\, \mathrm{d}t \tag{57}$$

around $\bar{A}$. So if we insert (56) into (55) we obtain

$$\bar{\sigma}^2(E, r) \sim \frac{8\pi^2}{\mathrm{vol}\,\Omega} \sum_{l=1}^{\infty} \left[\sigma_{\mathrm{cl}}^2(A_{2l}) + \sigma_{\mathrm{cl}}^2(B_{2l}) \right] [J_{2l}(r)]^2 \frac{1}{\sqrt{E}}. \tag{58}$$

A detailed study of the rate of quantum ergodicity in terms of the autocorrelation function, i.e. via equation (54), and a comparison with the semiclassical expectation (58) will be given in a separate paper.

5. Summary

We have discussed the autocorrelation function for eigenstates of quantum mechanical systems, and its relation to the behaviour of the classical system. For billiards we have derived a formula for the autocorrelation function of an eigenfunction in terms of the normal derivative on the boundary (10), which enables an efficient numerical computation.

Our main result is the correlation distance expansion of the autocorrelation function (28) for billiards, which provides an efficient expansion for small correlation distances, where only a small number of terms enters the sum. Moreover, it provides a tool for understanding the behaviour of the autocorrelation function for different types of eigenfunctions in terms of their semiclassical limit.

The coefficients in the correlation distance expansion (28) can be computed in terms of the radially integrated momentum density. Even though it is based on an approximation, our numerical study shows very good agreement with the corresponding exact results; only for large correlation distances do deviations become visible. As the expansion coefficients have to be determined just once for a given eigenfunction, this is also a numerically efficient method to compute the autocorrelation function. Similar, but more complicated, expansions can be derived in higher dimension and for more general systems (e.g. systems with potential and magnetic field), but then the Bessel functions have to be modified in order to reflect the structure of the energy shell of the classical system.

We applied the expansion of the autocorrelation function to different types of eigenfunctions, and showed that it provides a good tool for the understanding of their autocorrelation functions. In systems with mixed phase space regular states concentrated on tori and irregular states have been successfully treated. For chaotic system the fluctuations of the autocorrelation functions around the leading term are shown to be connected with the rate of quantum ergodicity. Moreover, by varying the correlation distance the autocorrelation function is shown to be an interesting new tool to measure the rate of quantum ergodicity on different length scales.

Acknowledgments

We would like to thank Professor Jonathan Keating for useful comments on the manuscript. AB acknowledges support by the Deutsche Forschungsgemeinschaft under contract no DFG-Ba 1973/1-1. RS acknowledges support by the Deutsche Forschungsgemeinschaft under contract no DFG-Ste 241/7-3.

Appendix A. Autocorrelation function in terms of normal derivatives on the boundary

We will give a derivation of the formula (10) which provides an expression of the autocorrelation function $C(\delta\boldsymbol{x})$ in terms of the normal derivative. Let $\psi(\boldsymbol{q})$ be a solution of the Helmholtz equation with Dirichlet boundary condition on $\partial\Omega$,

$$(\Delta + k^2)\psi(\boldsymbol{q}) = 0 \qquad \psi(\boldsymbol{q}) = 0 \qquad \text{for} \quad \boldsymbol{q} \in \partial\Omega \tag{59}$$

where we have defined $k = \sqrt{E}$, and let

$$u(s) := \boldsymbol{n}(s)\nabla\psi(\boldsymbol{q}(s)) \tag{60}$$

be the outer normal derivative of ψ on $\partial\Omega$, where s parametrizes $\partial\Omega$ in arclength. It is well known that

$$-\frac{1}{4}\int_{\partial\Omega} Y_0(k|\boldsymbol{q}-\boldsymbol{q}(s)|)u(s)\,\mathrm{d}s = \begin{cases}\psi(\boldsymbol{q}) & \text{for} \quad \boldsymbol{q} \in \Omega^\circ \\ 0 & \text{for} \quad \boldsymbol{q} \notin \Omega\end{cases} \tag{61}$$

and furthermore

$$\int_{\partial\Omega} J_0(k|\boldsymbol{q}-\boldsymbol{q}(s)|)u(s)\,\mathrm{d}s = 0. \tag{62}$$

Let $\rho(t)$ be a smooth cut-off function with

$$\rho(t) = \begin{cases}1 & \text{for} \quad t \leqslant 2\,\mathrm{diam}(\Omega) \\ 0 & \text{for} \quad t \geqslant 3\,\mathrm{diam}(\Omega)\end{cases} \tag{63}$$

where $\mathrm{diam}(\Omega)$ denotes the diameter of Ω. Then we have for $\boldsymbol{q}$ in some neighbourhood of Ω

$$\psi(\boldsymbol{q}) = -\frac{1}{4}\int_{\partial\Omega} \rho(k|\boldsymbol{q}-\boldsymbol{q}(s)|)Y_0(k|\boldsymbol{q}-\boldsymbol{q}(s)|)u(s)\,\mathrm{d}s \tag{64}$$

and obtain

$$C(\delta\boldsymbol{x}) = \int_{\mathbb{R}^2} \psi^*(\boldsymbol{q})\psi(\boldsymbol{q}+\delta\boldsymbol{x})\,\mathrm{d}q = \iint_{\partial\Omega\times\partial\Omega} K_\rho(\delta\boldsymbol{x}, s, s')u^*(s)u(s')\,\mathrm{d}s\,\mathrm{d}s' \tag{65}$$

with

$$\begin{aligned} K_\rho(\delta\boldsymbol{x}, s, s') &= \frac{1}{16}\int_{\mathbb{R}^2} \rho(k|\boldsymbol{q}-\boldsymbol{q}(s)|)Y_0(k|\boldsymbol{q}-\boldsymbol{q}(s)|)Y_0(k|\boldsymbol{q}-\boldsymbol{q}(s')+\delta\boldsymbol{x}|)\,\mathrm{d}q \\ &= \frac{1}{16}\int_{\mathbb{R}^2} \rho(k|\boldsymbol{q}|)Y_0(k|\boldsymbol{q}|)Y_0(k|\boldsymbol{q}+\boldsymbol{q}(s)-\boldsymbol{q}(s')+\delta\boldsymbol{x}|)\,\mathrm{d}q. \end{aligned} \tag{66}$$

Due to the factor $\rho(k|\boldsymbol{q}-\boldsymbol{q}(s)|)$ this integral is absolutely convergent. We now use Grafs addition theorem [45]

$$Y_0(k|\boldsymbol{q}+\Delta\boldsymbol{q}|) = \begin{cases}\sum_{l\in\mathbb{Z}} Y_l(k|\Delta\boldsymbol{q}|)J_l(k|\boldsymbol{q}|)\cos(l\varphi) & \text{for} \quad |\boldsymbol{q}| < |\Delta\boldsymbol{q}| \\ \sum_{l\in\mathbb{Z}} Y_l(k|\boldsymbol{q}|)J_l(k|\Delta\boldsymbol{q}|)\cos(l\varphi) & \text{for} \quad |\boldsymbol{q}| > |\Delta\boldsymbol{q}|\end{cases} \tag{67}$$

where $\Delta\boldsymbol{q} = \boldsymbol{q}(s) - \boldsymbol{q}(s') + \delta\boldsymbol{x}$ and φ is the angle between $\Delta\boldsymbol{q}$ and $\boldsymbol{q}$. Introducing polar coordinates in the integral in (66) and using (67) gives

$$K_\rho(\delta\boldsymbol{x}, s, s') = \frac{\pi}{8}\int_0^{|\Delta\boldsymbol{q}|} Y_0(kr)J_0(kr)r\,\mathrm{d}r\, Y_0(k|\Delta\boldsymbol{q}|) + \frac{\pi}{8}\int_{|\Delta\boldsymbol{q}|}^{\infty} \rho(kr)Y_0(kr)Y_0(kr)r\,\mathrm{d}r\, J_0(k|\Delta\boldsymbol{q}|) \tag{68}$$

where we have furthermore used that $\rho(r) = 1$ for $r \leqslant |\Delta\boldsymbol{q}|$ by (63). The first integral is

$$\int_0^{|\Delta\boldsymbol{q}|} Y_0(kr)J_0(kr)r\,\mathrm{d}r = \frac{|\Delta\boldsymbol{q}|^2}{2}[Y_0(k|\Delta\boldsymbol{q}|)J_0(k|\Delta\boldsymbol{q}|) + Y_1(k|\Delta\boldsymbol{q}|)J_1(k|\Delta\boldsymbol{q}|)] \tag{69}$$

see, e.g. [45], and for the second one partial integration gives

$$\int_{|\Delta\boldsymbol{q}|}^{\infty} \rho(kr)Y_0(kr)Y_0(kr)r\,\mathrm{d}r = -\frac{|\Delta\boldsymbol{q}|^2}{2}[Y_0(k|\Delta\boldsymbol{q}|)Y_0(k|\Delta\boldsymbol{q}|) + Y_1(k|\Delta\boldsymbol{q}|)Y_1(k|\Delta\boldsymbol{q}|)] - \frac{k}{2}\int_{|\Delta\boldsymbol{q}|}^{\infty} \rho'(kr)[Y_0(kr)Y_0(kr) + Y_1(kr)Y_1(kr)]r^2\,\mathrm{d}r. \tag{70}$$

Note that since ρ' has compact support the second integral is over a finite interval, and for $s, s' \in \partial\Omega$, $\delta\boldsymbol{x} \in \Omega$ the lower limit of the integral, $|\Delta\boldsymbol{q}|$, is outside the support of ρ', hence the second term on the right-hand side of equation (70) is constant. So we get

$$K_\rho(\delta\boldsymbol{x}, s, s') = K(\delta\boldsymbol{x}, s, s') + R_\rho(\delta\boldsymbol{x}, s, s') \tag{71}$$

with

$$K(\delta\boldsymbol{x}, s, s') = \frac{\pi|\Delta\boldsymbol{q}|^2}{16}[Y_1(k|\Delta\boldsymbol{q}|)J_1(k|\Delta\boldsymbol{q}|)Y_0(k|\Delta\boldsymbol{q}|) - Y_1(k|\Delta\boldsymbol{q}|)Y_1(k|\Delta\boldsymbol{q}|)J_0(k|\Delta\boldsymbol{q}|)] \tag{72}$$

and

$$R_\rho(\delta\boldsymbol{x}, s, s') = C\,J_0(k|\Delta\boldsymbol{q}|) \tag{73}$$

with C constant and by (62) this term gives no contribution to $C(\delta\boldsymbol{x})$. Using a Wronsky determinant of Bessel functions [45] we can simplify $K(\delta\boldsymbol{x}, s, s')$ further

$$K(\delta\boldsymbol{x}, s, s') = \frac{\pi|\Delta\boldsymbol{q}|^2}{16}Y_1(k|\Delta\boldsymbol{q}|)[J_1(k|\Delta\boldsymbol{q}|)Y_0(k|\Delta\boldsymbol{q}|) - Y_1(k|\Delta\boldsymbol{q}|)J_0(k|\Delta\boldsymbol{q}|)] = \frac{\pi|\Delta\boldsymbol{q}|^2}{16}Y_1(k|\Delta\boldsymbol{q}|)\frac{2}{\pi k|\Delta\boldsymbol{q}|} = \frac{|\Delta\boldsymbol{q}|}{8k}Y_1(k|\Delta\boldsymbol{q}|) \tag{74}$$

which gives the final result.

Appendix B. Remainder estimate

In this appendix we sketch the derivation of the remainder estimate in equation (19). We start by representing the integral as an expectation value, see (24)

$$\int_0^\infty\int_0^{2\pi}\int_\Omega \rho(\boldsymbol{x}-\boldsymbol{q})W(\boldsymbol{p},\boldsymbol{q})\,\mathrm{d}q'\,\mathrm{e}^{\mathrm{i}r|\delta\boldsymbol{x}|\cos(\varphi-\theta)/\sqrt{E}}\,r\,\mathrm{d}\varphi\,\mathrm{d}r = \langle\psi, A\psi\rangle \tag{75}$$

where A is the Weyl quantization of the symbol

$$a(\boldsymbol{p},\boldsymbol{q}) := \rho(\boldsymbol{x}-\boldsymbol{q})\,\mathrm{e}^{\mathrm{i}\frac{|\boldsymbol{p}|}{\sqrt{E}}|\delta\boldsymbol{x}|\cos(\varphi-\theta)}. \tag{76}$$

The basic idea is to find a decomposition of the operator A

$$A = A_0 + (\sqrt{-\Delta} - \sqrt{E})A_1 + R \tag{77}$$

where A_0 has the Weyl symbol

$$a_0(\boldsymbol{p},\boldsymbol{q}) = \rho(\boldsymbol{x}-\boldsymbol{q})\,\mathrm{e}^{\mathrm{i}|\delta\boldsymbol{x}|\cos(\varphi-\theta)} \tag{78}$$

and the remainder R satisfies

$$\|R\| \leqslant C\,E^{-1/2}. \tag{79}$$

If we assume the decomposition (77) and take the expectation value of both sides, one gets

$$\langle\psi, A\psi\rangle = \langle\psi, A_0\psi\rangle + \langle\psi, R\psi\rangle \tag{80}$$

where $(\sqrt{-\Delta}-\sqrt{E})\psi = 0$ has been used. In terms of the symbols equation (80) is the desired result, see (19)

$$\int_0^\infty\int_0^{2\pi}\int_\Omega W(\boldsymbol{p},\boldsymbol{q})\rho(\boldsymbol{x}-\boldsymbol{q})\,\mathrm{d}q'\,\mathrm{e}^{\mathrm{i}r|\delta\boldsymbol{x}|\cos(\varphi-\theta)/\sqrt{E}}\,r\,\mathrm{d}\varphi\,\mathrm{d}r$$
$$= \int_0^\infty\int_0^{2\pi}\int_\Omega W(\boldsymbol{p},\boldsymbol{q})\rho(\boldsymbol{x}-\boldsymbol{q})\,\mathrm{d}q'\,\mathrm{e}^{\mathrm{i}|\delta\boldsymbol{x}|\cos(\varphi-\theta)/}\,r\,\mathrm{d}\varphi\,\mathrm{d}r + O(rE^{-1/2}). \tag{81}$$

Let us now show that the decomposition (77) is basically a quantization of the Taylor expansion of the symbol $a(\boldsymbol{p},\boldsymbol{q})$ around $|\boldsymbol{p}| = \sqrt{E}$,

$$a(\boldsymbol{p},\boldsymbol{q}) = a_0(\boldsymbol{p},\boldsymbol{q}) + (|\boldsymbol{p}|-\sqrt{E})a_1(\boldsymbol{p},\boldsymbol{q}). \tag{82}$$

Quantizing this classical decomposition yields (77) with R given as the Weyl quantization of

$$r(\boldsymbol{p},\boldsymbol{q}) = (|\boldsymbol{p}|-\sqrt{E})a_1(\boldsymbol{p},\boldsymbol{q}) - (|\boldsymbol{p}|-\sqrt{E})\#a_1(\boldsymbol{p},\boldsymbol{q}) \tag{83}$$

since the Weyl symbol of $(\sqrt{-\Delta}-\sqrt{E})A_1$ is $(|\boldsymbol{p}|-\sqrt{E})\#a_1(\boldsymbol{p},\boldsymbol{q})$ with # denoting the symbol product (see e.g. [46]). Since E is a constant we have

$$r(\boldsymbol{p},\boldsymbol{q}) = |\boldsymbol{p}|a_1(\boldsymbol{p},\boldsymbol{q}) - |\boldsymbol{p}|\#a_1(\boldsymbol{p},\boldsymbol{q}) \tag{84}$$

and this is a function which is bounded and of order $O(|\delta\boldsymbol{x}|E^{-1/2})$, and all its derivatives are bounded and of order $O(|\delta\boldsymbol{x}|E^{-1/2})$, too. So by the Calderon Vallaincourt theorem [46] the estimate (79) follows.

Appendix C. Estimating the Bessel sum

In this appendix we determine how many terms in the sum (28) have to be taken into account such that the remainder is smaller than some given error δ. From (26) and (27) it follows that for fixed ψ

$$|\langle\psi, \hat{A}_{2l}(\boldsymbol{x})\psi\rangle\cos(2l\theta) + \langle\psi, \hat{B}_{2l}(\boldsymbol{x})\psi\rangle\sin(2l\theta)| \leqslant C. \tag{85}$$

Thus if we split the sum

$$\sum_{l=1}^{\infty}(-1)^l[\langle\psi, \hat{A}_{2l}(\boldsymbol{x})\psi\rangle\cos(2l\theta) + \langle\psi, \hat{B}_{2l}(\boldsymbol{x})\psi\rangle\sin(2l\theta)]\,J_{2l}(|\delta\boldsymbol{x}|)$$
$$= \sum_{l=1}^{m-1}(-1)^l[\langle\psi, \hat{A}_{2l}(\boldsymbol{x})\psi\rangle\cos(2l\theta) + \langle\psi, \hat{B}_{2l}(\boldsymbol{x})\psi\rangle\sin(2l\theta)]\,J_{2l}(|\delta\boldsymbol{x}|) + R_m(|\delta\boldsymbol{x}|) \tag{86}$$

we get for the remainder

$$|R_m(r)| \leqslant C\sum_{l=m}^{\infty}|J_{2l}(r)|. \tag{87}$$

Therefore we have to estimate the sum over Bessel functions

$$\sum_{l=m}^{\infty} |J_{2l}(r)| \tag{88}$$

and determine its dependence on m and r. The asymptotics in the transition region

$$J_{2l}(2l - z(2l)^{1/3}) \sim \frac{1}{l^{1/3}} \operatorname{Ai}(2^{1/3}z) \tag{89}$$

gives that $J_{2l}(r)$ is monotonically increasing for $r < 2l$, such that for $r < 2m$

$$\sum_{l=m}^{\infty} |J_{2l}(r)| = \sum_{l=m}^{\infty} \frac{1}{l^{1/3}} \operatorname{Ai}\left(\frac{2l - r}{l^{1/3}}\right) + O(m^{-1}). \tag{90}$$

Defining z by

$$r = 2m - zm^{1/3} \tag{91}$$

we obtain

$$\begin{aligned}\sum_{l=m}^{\infty} \frac{1}{l^{1/3}} \operatorname{Ai}\left(\frac{2l - r}{l^{1/3}}\right) &= \sum_{l=m}^{\infty} \frac{1}{l^{1/3}} \operatorname{Ai}\left(\frac{2(l-m)}{l^{1/3}} + z\left(\frac{m}{l}\right)^{1/3}\right) \\ &= \sum_{l=0}^{\infty} \frac{1}{(l+m)^{1/3}} \operatorname{Ai}\left(\frac{2l}{(l+m)^{1/3}} + z\left(\frac{m}{l+m}\right)^{1/3}\right) \\ &= \sum_{l=0}^{\infty} \frac{1}{m^{1/3}} \operatorname{Ai}\left(\frac{2l}{m^{1/3}} + z\right) + O(m^{-1/3})\end{aligned} \tag{92}$$

where we have furthermore used that for large m only the terms with $l \ll m$ contribute, because the Airy function is exponentially decreasing for positive arguments. The Euler McLaurin formula then gives

$$\begin{aligned}\sum_{l=0}^{\infty} \frac{1}{m^{1/3}} \operatorname{Ai}\left(\frac{2l}{m^{1/3}} + z\right) &= \int_0^{\infty} \frac{1}{m^{1/3}} \operatorname{Ai}\left(\frac{2l}{m^{1/3}} + z\right) \mathrm{d}l + O(m^{-1/3}) \\ &= \frac{1}{2} \int_z^{\infty} \operatorname{Ai}(x)\, \mathrm{d}x + O(m^{-1/3}).\end{aligned} \tag{93}$$

And so finally we arrive at

$$\sum_{l=m}^{\infty} |J_{2l}(r)| = \frac{1}{2} \int_z^{\infty} \operatorname{Ai}(x)\ \mathrm{d}x + O(m^{-1/3}). \tag{94}$$

The function $\int_z^{\infty} \operatorname{Ai}(x)\ \mathrm{d}x$ is monotonically decreasing, so for a given $\delta > 0$ we can define a $z(\delta)$ by

$$\frac{1}{2} \int_{z(\delta)}^{\infty} \operatorname{Ai}(x)\ \mathrm{d}x = \delta \tag{95}$$

and then (91) defines together with (95) a function $m(r, \delta)$ such that

$$\sum_{l=[m(r,\delta)+1]}^{\infty} |J_{2l}(r)| = \delta + O(r^{-1/3}). \tag{96}$$

By solving (91) for large r, we see that we have to take approximately

$$m(r, \delta) \sim \frac{r}{2} + \frac{z}{2}\left(\frac{r}{2}\right)^{1/3} \tag{97}$$

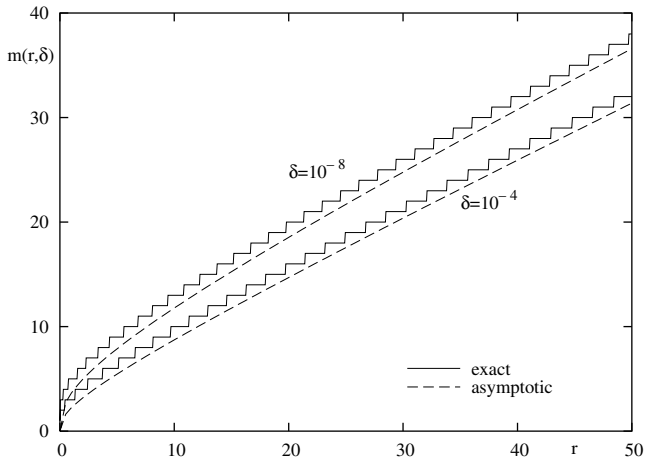

Figure 12. For the bounds $\delta = 10^{-4}$ and $\delta = 10^{-8}$ of the sum over Bessel functions (88) the result of the exact computation of $m(r, \delta)$ (full curves) and the asymptotic result (97) are compared. The asymptotic result approaches the exact one slowly from below with a rate $O(r^{-1/3})$.

terms in the sum (28) over l into account such that the error is $\delta + O(r^{-1/3})$.

For instance, if we require $\delta = 10^{-4}$, then (95) gives $z(\delta) = 4.359\ldots$; for $\delta = 10^{-8}$ one gets $z(\delta) = 7.925\ldots$. In figure 12 we show for these choices of z the asymptotic result (97) compared to the exact computation, corresponding to (88). The asymptotic result approaches the exact one slowly from below; in the plotted region a constant offset by two compared to (97) gives a good bound for $m(r, \delta)$.

References

[1] Berry M V 1977 Regular and irregular semiclassical wavefunctions *J. Phys. A: Math. Gen.* **10** 2083
[2] McDonald S W and Kaufmann A N 1988 Wave chaos in the stadium: statistical properties of short-wave solutions of the Helmholtz equation *Phys. Rev.* A **37** 3067
[3] Aurich R and Steiner F 1993 Statistical properties of highly excited quantum eigenstates of a strongly chaotic system *Physica* D **64** 185
[4] Li B and Robnik M 1994 Statistical properties of high-lying chaotic eigenstates *J. Phys. A: Math. Gen.* **27** 5509
[5] Robert D 1998 Semi-classical approximation in quantum mechanics. A survey of old and recent mathematical results *Helv. Phys. Acta* **71** 44
[6] Shnirelman A I 1974 Ergodic properties of eigenfunctions *Usp. Math. Nauk* **29** 181 (in Russian)
[7] Zelditch S 1987 Uniform distribution of eigenfunctions on compact hyperbolic surfaces *Duke. Math. J.* **55** 919
[8] Colin de Verdiére Y 1985 Ergodicité et fonctions propres du laplacien *Commun. Math. Phys.* **102** 497 (in French)
[9] Helffer B, Martinez A and Robert D 1987 Ergodicité et limite semi-classique *Commun. Math. Phys.* **109** 313 (in French)
[10] Gérard P and Leichtnam E 1993 Ergodic properties of eigenfunctions for the Dirichlet problem *Duke Math. J.* **71** 559
[11] Zelditch S and Zworski M 1996 Ergodicity of eigenfunctions for ergodic billiards *Commun. Math. Phys.* **175** 673
[12] Bäcker A, Schubert R and Stifter P 1998 Rate of quantum ergodicity in Euclidean billiards *Phys. Rev.* E **57** 5425
Bäcker A, Schubert R and Stifter P 1998 *Phys. Rev.* E **58** 5192 (erratum)
[13] Voros A 1976 Semi–classical approximations *Ann. Inst. H Poincaré* A **24** 31
[14] Voros A 1977 Asymptotic $\hbar$–expansions of stationary quantum states *Ann. Inst. H Poincaré* A **26** 343
[15] Berry M V 1983 Semiclassical mechanics of regular and irregular motion *Comportement Chaotique des Systémes Déterministes—Chaotic Behaviour of Deterministic Systems* ed G Iooss, R H G Hellemann and R Stora (Amsterdam: North-Holland) pp 171–271
[16] Srednicki M and Stiernelof F 1996 Gaussian fluctuations in chaotic eigenstates *J. Phys. A: Math. Gen.* **29** 5817

[17] Srednicki M 1996 Gaussian random eigenfunctions and spatial correlations in quantum dots *Phys. Rev.* E **54** 954
[18] Hortikar S and Srednicki M 1998 Correlations in chaotic eigenfunctions at large separation *Phys. Rev. Lett.* **80** 1646
[19] Hortikar S and Srednicki M 1998 Random matrix elements and eigenfunctions in chaotic systems *Phys. Rev.* E **57** 7313
[20] Gornyi I V and Mirlin A D 2001 Wave function correlations on the ballistic scale: Exploring quantum chaos by quantum disorder *Preprint* cond-mat/0105103
[21] Li B and Rouben D C 2001 Correlations of chaotic eigenfunctions: a semiclassical analysis *J. Phys. A: Math. Gen.* **34** 7381
[22] Toscano F and Lewenkopf C H 2001 Semiclassical spatial correlations in chaotic wave functions *Preprint* nlin.CD/0108032
[23] Shapiro M and Goelman G 1984 Onset of chaos in an isolated energy eigenstate *Phys. Rev. Lett.* **53** 1714
[24] Shapiro M, Ronkin J and Brumer P 1988 Scaling laws and correlation length of quantum and classical ergodic states *Chem. Phys. Lett.* **148** 177
[25] Veble G, Robnik M and Liu J 1999 Study of regular and irregular states in generic systems *J. Phys. A: Math. Gen.* **32** 6423
[26] Schubert R 2001 Semiclassical localization in phase space *PhD Thesis* Abteilung Theoretische Physik, Universität Ulm
[27] Bunimovich L A 1974 On ergodic properties of certain billiards *Funct. Anal. Appl.* **8** 254
[28] Bunimovich L A 1979 On the ergodic properties of nowhere dispersing billiards *Commun. Math. Phys.* **65** 295
[29] Robnik M 1983 Classical dynamics of a family of billiards with analytic boundaries *J. Phys. A: Math. Gen.* **16** 3971
[30] Robnik M 1984 Quantising a generic family of billiards with analytic boundaries *J. Phys. A: Math. Gen.* **17** 1049
[31] Wojtkowski M 1986 Principles for the design of billiards with nonvanishing Lyapunov exponents *Commun. Math. Phys.* **105** 391
[32] Szász D 1992 On the K-property of some planar hyperbolic billiards *Commun. Math. Phys.* **145** 595
[33] Markarian R 1993 New ergodic billiards: exact results *Nonlinearity* **6** 819
[34] Prosen T and Robnik M Private communication
[35] Prosen T and Robnik M 1993 Energy level statistics in the transition region between integrability and chaos *J. Phys. A: Math. Gen.* **26** 2371
[36] Riddel R J Jr 1979 Boundary-distribution solution of the Helmholtz equation for a region with corners *J. Comput. Phys.* **31** 21
[37] Berry M V and Wilkinson M 1984 Diabolical points in the spectra of triangles *Proc. R. Soc.* A **392** 15
[38] Bäcker A 1998 Classical and quantum chaos in billiards *PhD Thesis* Abteilung Theoretische Physik, Universität Ulm
[39] Vergini E and Saraceno M 1995 Calculation of highly excited states of billiards *Phys. Rev.* E **52** 2204
[40] Heller E J 1984 Bound-state eigenfunctions of classically chaotic Hamiltonian systems: scars of periodic orbits *Phys. Rev. Lett.* **53** 1515
[41] Bai Y Y, Hose G, Stefański K and Taylor H S 1985 Born–Oppenheimer adiabatic mechanism for regularity of states in the quantum stadium billiard *Phys. Rev.* A **31** 2821
[42] O'Connor P W and Heller E J 1988 Quantum localization for a strongly classically chaotic system *Phys. Rev. Lett.* **61** 2288
[43] Tanner G 1997 How chaotic is the stadium billiard? A semiclassical analysis *J. Phys. A: Math. Gen.* **30** 2863
[44] Bäcker A, Schubert R and Stifter P 1997 On the number of bouncing-ball modes in billiards *J. Phys. A: Math. Gen.* **30** 6783
[45] Abramowitz M and Stegun I A (eds) 1984 *Pocketbook of Mathematical Functions* (Thun–Frankfurt/Main: Deutsch) abridged edition
[46] Folland G B 1989 *Harmonic Analysis in Phase Space (Annals of Mathematics Studies vol 122)* (Princeton: Princeton University Press)
[47] Zyczkowski K 1992 Classical and quantum billiards, integrable, nonintegrable, and pseudo-integrable *Acta Phys. Pol.* B **23** 245
[48] Bäcker A and Schubert R 1999 Chaotic eigenfunctions in momentum space *J. Phys. A: Math. Gen.* **32** 4795
[49] Tualle J M and Voros A 1995 Normal modes of billiards portrayed in the stellar (or nodal) representation, *Chaos, Solitons Fractals* **5** 1085
[50] Simonotti F P, Vergini E and Saraceno M 1997 Quantitative study of scars in the boundary section of the stadium billiard *Phys. Rev.* E **56** 3859

[51] Bäcker A and Schubert R 2002 Amplitude distribution of eigenfunctions in mixed systems *J. Phys. A: Math. Gen.* **35** 527 (preceding paper) (nlin.CD/0106017)
[52] Percival I C 1973 Regular and irregular spectra *J. Phys. B: At. Mol. Phys.* **6** L229
[53] Bohigas O, Tomsovic S and Ullmo D 1990 Dynamical quasidegeneracies and separation of regular and irregular quantum levels *Phys. Rev. Lett.* **64** 1479
[54] Prosen T and Robnik M 1993 Survey of the eigenfunctions of a billiard system between integrability and chaos *J. Phys. A: Math. Gen.* **26** 5365
[55] Li B and Robnik M 1995 Separating the regular and irregular energy levels and their statistics in a Hamiltonian system with mixed classical dynamics *J. Phys. A: Math. Gen.* **28** 4843
[56] Li B and Robnik M 1995 Geometry of high-lying eigenfunctions in a plane billiard system having mixed-type classical dynamics *J. Phys. A: Math. Gen.* **28** 2799
[57] Carlo G, Vergini E and Fendrik A 1998 Numerical verification of Percival's conjecture in a quantum billiard *Phys. Rev.* E **57** 5397 (chao-dyn/9804016)
[58] Eckhardt B, Fishman S, Keating J, Agam O, Main J and Müller K 1995 Approach to ergodicity in quantum wave functions *Phys. Rev.* E **52** 5893